iScience

CellPress

Article

Necroptosis of Intestinal Epithelial Cells Induces Type 3 Innate Lymphoid Cell-Dependent Lethal Ileitis

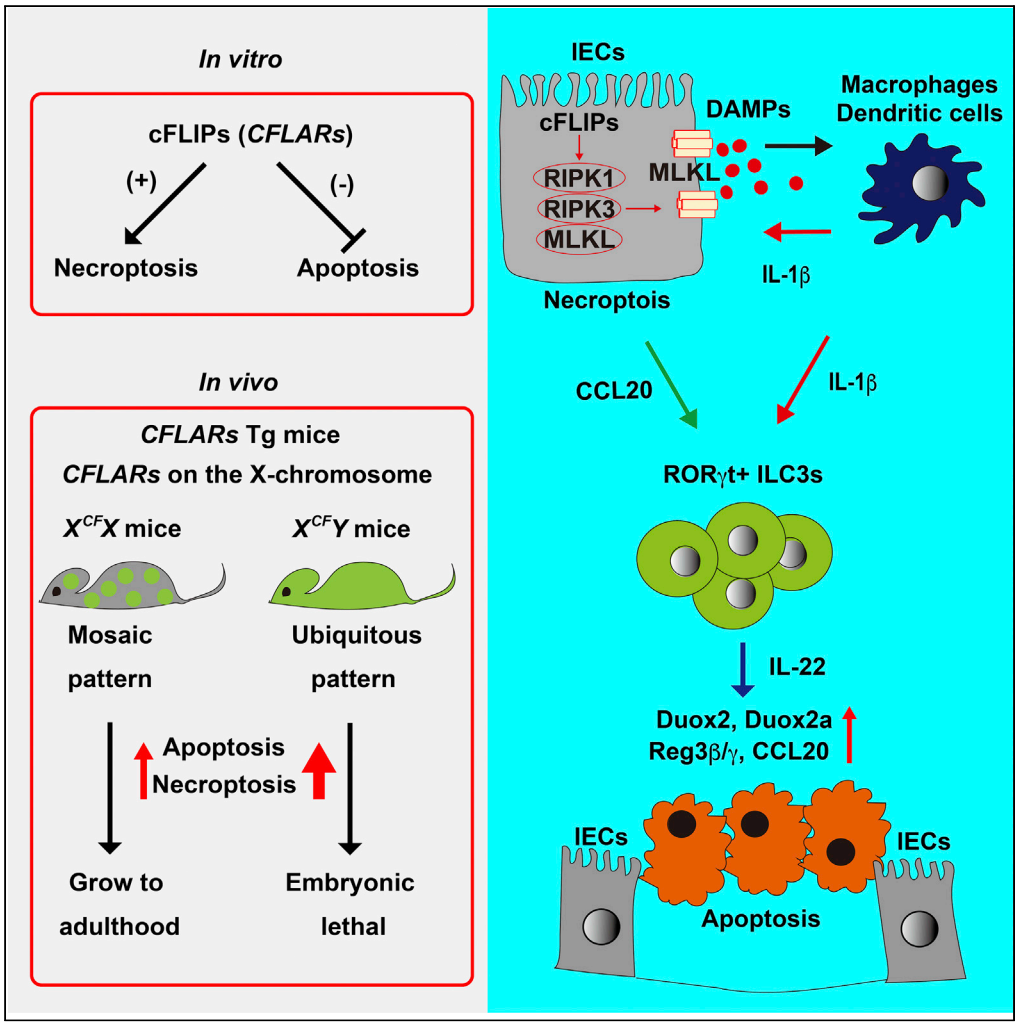

Ryodai Shindo, Masaki Ohmuraya, Sachiko Komazawa-Sakon, ..., Kenta Moriwaki, Kimi Araki, Hiroyasu Nakano

hiroyasu.nakano@med.toho-u.ac.jp

HIGHLIGHTS

CFLARs Tg mice develop severe ileitis *in utero*

Intestinal epithelial cells die by apoptosis and necroptosis in *CFLARs* Tg mice

Blockade of necroptosis rescues lethality of *CFLARs* Tg mice

Necroptosis activates type 3 innate lymphoid cells, resulting in severe ileitis

Shindo et al., iScience *15*, 536–551
May 31, 2019
https://doi.org/10.1016/j.isci.2019.05.011

iScience

CellPress

Article

Necroptosis of Intestinal Epithelial Cells Induces Type 3 Innate Lymphoid Cell-Dependent Lethal Ileitis

Ryodai Shindo,[1] Masaki Ohmuraya,[2] Sachiko Komazawa-Sakon,[1] Sanae Miyake,[1] Yutaka Deguchi,[1] Soh Yamazaki,[1] Takashi Nishina,[1] Takayuki Yoshimoto,[3] Soichiro Kakuta,[4] Masato Koike,[5] Yasuo Uchiyama,[4] Hiroyuki Konishi,[6] Hiroshi Kiyama,[6] Tetuo Mikami,[7] Kenta Moriwaki,[8] Kimi Araki,[9] and Hiroyasu Nakano[1,10,11,*]

SUMMARY

A short form of cellular FLICE-inhibitory protein encoded by *CFLARs* promotes necroptosis. Although necroptosis is involved in various pathological conditions, the detailed mechanisms are not fully understood. Here we generated transgenic mice wherein *CFLARs* was integrated onto the X chromosome. All male *CFLARs* Tg mice died perinatally due to severe ileitis. Although necroptosis was observed in various tissues of *CFLARs* Tg mice, large numbers of intestinal epithelial cells (IECs) died by apoptosis. Deletion of *Ripk3* or *Mlkl*, essential genes of necroptosis, prevented both necroptosis and apoptosis, and rescued lethality of *CFLARs* Tg mice. Type 3 innate lymphoid cells (ILC3s) were activated and recruited to the small intestine along with upregulation of *interleukin-22* (*Il22*) in *CFLARs* Tg mice. Deletion of ILC3s or *Il22* rescued lethality of *CFLARs* Tg mice by preventing apoptosis, but not necroptosis of IECs. Together, necroptosis-dependent activation of ILC3s induces lethal ileitis in an IL-22-dependent manner.

INTRODUCTION

Apoptosis is the prototype of programmed cell death or regulated cell death and is executed by sequential activation of cysteine proteases, named *caspases* (Riedl and Salvesen, 2007; Yuan, 2006). Recent studies have reported another form of regulated cell death, which is also referred to as necroptosis (Christofferson and Yuan, 2010). Activation of death receptors induced by cognate death ligands including tumor necrosis factor (TNF), Fas, and TRAIL triggers the formation of death-inducing signaling complex, termed complex IIb, that is composed of Fas-associated protein with death domain (FADD), receptor-interacting protein kinase (RIPK)1, RIPK3, and caspase 8 (Pasparakis and Vandenabeele, 2015). Once caspase 8 is activated, it subsequently activates downstream caspases 3, 6, and 7, resulting in the execution of apoptosis. Activation of caspase 8 normally suppresses the execution of necroptosis by inactivating RIPK1 and CYLD (Chan et al., 2003; O'Donnell et al., 2011). In sharp contrast, in the presence of either caspase inhibitors, or deletion of *Fadd* or *Caspase 8*, the complex IIb evolves into the necrosome that is composed of RIPK1, RIPK3, and mixed lineage kinase domain-like (MLKL). Sequential phosphorylation of RIPK1, RIPK3, and MLKL results in oligomerization and subsequent plasma membrane translocation of MLKL, resulting in membrane permeabilization and necroptosis (Pasparakis and Vandenabeele, 2015). Necroptosis is induced by death ligands, polyinosinic:polycytidylic acid, and viral infection and is involved in various pathological conditions including drug-induced pancreatitis, ischemic reperfusion injury, and elimination of some types of viruses (Weinlich et al., 2017). Taken that germline deletion of *Fadd* and *Caspase 8* results in embryonic lethality due to an increase in necroptosis (Kaiser et al., 2011; Oberst et al., 2011; Zhang et al., 2011), the FADD/caspase 8-dependent apoptotic pathway normally suppresses the necroptotic pathway during normal development. However, an interplay between apoptosis and necroptosis *in vivo* is not fully understood.

Cellular FLICE-inhibitory protein (cFLIP) is a catalytically inactive homolog of the initiator caspase, caspase 8, and blocks cell death induced by death ligands (Budd et al., 2006; Nakano et al., 2017). We and others have generated conditional *Cflar*-deficient mice and reported that cFLIP plays a crucial role in preventing cells from apoptosis and necroptosis (Dillon et al., 2012; Panayotova-Dimitrova et al., 2013; Piao et al., 2012, 2018; Schattenberg et al., 2011; Zhang and He, 2005). *CFLAR* gene encodes two proteins, designated as long form ($cFLIP_L$) and short form (cFLIPs) due to alternative splicing. Intriguingly, recent studies have shown that $cFLIP_L$ blocks both apoptosis and necroptosis, whereas cFLIPs blocks apoptosis but promotes

[1]Department of Biochemistry, Toho University School of Medicine, 5-21-16 Omori-Nishi, Ota-ku, Tokyo 143-8540, Japan

[2]Department of Genetics, Hyogo College of Medicine, Nishinomiya, Hyogo 663-8501, Japan

[3]Department of Immunoregulation, Institute of Medical Science, Tokyo Medical University, 6-1-1 Shinjuku-ku, Tokyo 160-8402, Japan

[4]Department of Cellular Molecular Neuropathology, Juntendo University Graduate School of Medicine, 2-1-1 Hongo, Bunkyo-ku, Tokyo 113-8421, Japan

[5]Department of Cell Biology and Neuroscience, Juntendo University Graduate School of Medicine, 2-1-1 Hongo, Bunkyo-ku, Tokyo 113-8421, Japan

[6]Department of Functional Anatomy and Neuroscience, Graduate School of Medicine, Nagoya University, 65 Tsurumaicho, Showa-ku, Nagoya 466-8560, Japan

[7]Department of Pathology, Toho University School of Medicine, 5-21-16 Omori-Nishi, Ota-ku, Tokyo 143-8540, Japan

[8]Department of Cell Biology, Osaka University Graduate School of Medicine, 2-2 Yamadaoka, Suita, Osaka 565-0871, Japan

[9]Institute of Resource Development and Analysis, Kumamoto University, 2-2-1 Honjo, Chuo-ku, Kumamoto 860-0811, Japan

[10]Host Defense Research Center, Toho University

Continued

necroptosis (Feoktistova et al., 2011; Oberst et al., 2011). However, it is unclear whether the expression of cFLIPs promotes necroptosis *in vivo*, and the consequences of cFLIPs-dependent necroptosis are largely unknown.

Tissue homeostasis of the intestine is regulated by epithelial cells and various types of immune cells, including dendritic cells, macrophages, B and T cells, and innate lymphoid cells (Honda and Littman, 2016; Maloy and Powrie, 2011). Among them, T_H17 cells and type 3 innate lymphoid cells (ILC3s) play a crucial role in preventing infection of the intestine from pathogenic bacteria (Ohnmacht, 2016; Vivier et al., 2018). The development of T_H17 cells and ILC3s totally depends on the *Rorc* gene that encodes RAR-related orphan receptor gamma t (RORγt) protein. Under normal conditions, various stimuli such as colonization of commensal bacteria, food-derived metabolites, and cytokines activate macrophages or dendritic cells, resulting in the production of interleukin (IL)-23 and IL-1β (Manta et al., 2013; Mortha et al., 2014). IL-23 and IL-1β subsequently activate T_H17 cells and ILC3s. IL-22 produced by activated ILC3s plays a dominant role in maintaining intestinal homeostasis and controls a set of genes showing antimicrobial activities, such as *Regenerating islet-derived protein (Reg)3b* and *Reg3*g (Eidenschenk et al., 2014; Parks et al., 2015). In sharp contrast, aberrantly activated ILC3s produce excessive amounts of IL-22, resulting in intestinal tissue injury under certain conditions including injection of anti-CD40 antibody, immaturity of acquired immunity, absence of regulatory T (Treg) cells, or transgenic expression of *Il23* (Bauche et al., 2018; Buonocore et al., 2010; Chen et al., 2015). However, the mechanism underlying aberrant activation of ILC3s and ILC3-dependent tissue injury are not fully understood.

X chromosome inactivation is a process in which one of the two X chromosomes is randomly inactivated in female mammalian cells (Lyon, 1971). Hence integration of gene *A* onto one allele of two X chromosomes results in a mosaic pattern expression of gene *A* due to random inactivation of X chromosome. During generation of a promoter trap library, we obtained one ES line, designated *B210*, where a trap vector was integrated into the *Diap2* locus on the X chromosome (Taniwaki et al., 2005). Using B210 ES line, we previously reported that mice harboring human *SPINK1* gene in the *Diap2* locus expressed human SPINK1 in a mosaic pattern (Sakata et al., 2016). This strategy might be useful to express cell death-promoting gene in mice by preventing potentially embryonic lethal phenotype.

To further understand the consequences of necroptosis and an interplay between apoptosis and necroptosis *in vivo*, we generated *CFLARs* Tg mice wherein the *CFLARs* gene was specifically integrated onto the X chromosome. Male and female *CFLARs* Tg mice were referred to as $X^{CF}Y$ and $X^{CF}X$ mice, respectively. All $X^{CF}Y$ mice died *in utero* due to severe ileitis. Immunohistochemistry (IHC) with anti-phosphorylated RIPK3 (pRIPK3) antibody and transmission electron microscopy (TEM) revealed that a number of intestinal epithelial cells (IECs) died by necroptosis. Unexpectedly, large numbers of IECs died by apoptosis in the SI of *CFLARs* Tg mice. Surprisingly, deletion of *Ripk3* or *Mlkl* rescued embryonic lethality of *CFLARs* Tg mice by preventing not only necroptosis but also apoptosis of IECs. Moreover, deletion of *Rorc* or *Il22* prevented lethal ileitis in *CFLARs* Tg mice by preventing apoptosis, but not necroptosis of IECs. Together, necroptosis of IECs activated ILC3s, which further induced apoptosis of IECs in an IL-22-dependent manner.

RESULTS

CFLARs Transgenic Mice Die Perinatally

To circumvent embryonic lethality potentially induced by overexpression of cFLIPs in mice, we generated *CFLARs* Tg mice by utilizing X chromosome inactivation (Figure 1A). As we assumed that $X^{CF}Y$ mice might be embryonic lethal, we performed timed mating. $X^{CF}Y$ mice developed normally until embryonic day embryonic day (E) 16.5 but began to die at E17.5 to E18.5, and the rest of $X^{CF}Y$ mice died at birth (Figure 1B). Only 10% of $X^{CF}X$ mice died perinatally, but the other $X^{CF}X$ mice survived until adulthood. Although cFLIPs were expressed in various tissues (Figure 1C), an apparent histological abnormality was restricted to the small intestine (SI) (Figure S1A). The intestinal lumen was mostly occupied with villous structure in the SI of wild-type embryos, whereas the lumen was dilated and the length of villi was severely shortened in $X^{CF}Y$ mice, and to a lesser extent, in $X^{CF}X$ mice at E18.5 (Figure 1D). IECs were detached from villi and accumulated in the lumen of the SI of $X^{CF}Y$ mice. Surprisingly, IECs in the lumen and a few IECs in villi were positive for cleaved caspase (CC) 3 staining, suggesting that these IECs died by apoptosis (Figure 1E). Consistently, CC3 was also detected in tissue extracts of the SI of *CFLARs* Tg mice at E18.5 (Figure 1F). We also found that large numbers of cells were positive for TUNEL staining in the lumen of the SI of $X^{CF}Y$ mice, and to a lesser extent, in $X^{CF}X$ mice at E18.5 (Figure 1G).

School of Medicine, 5-21-16 Omori-Nishi, Ota-ku, Tokyo 143-8540, Japan

[11]Lead Contact

*Correspondence: hiroyasu.nakano@med.toho-u.ac.jp

https://doi.org/10.1016/j.isci.2019.05.011

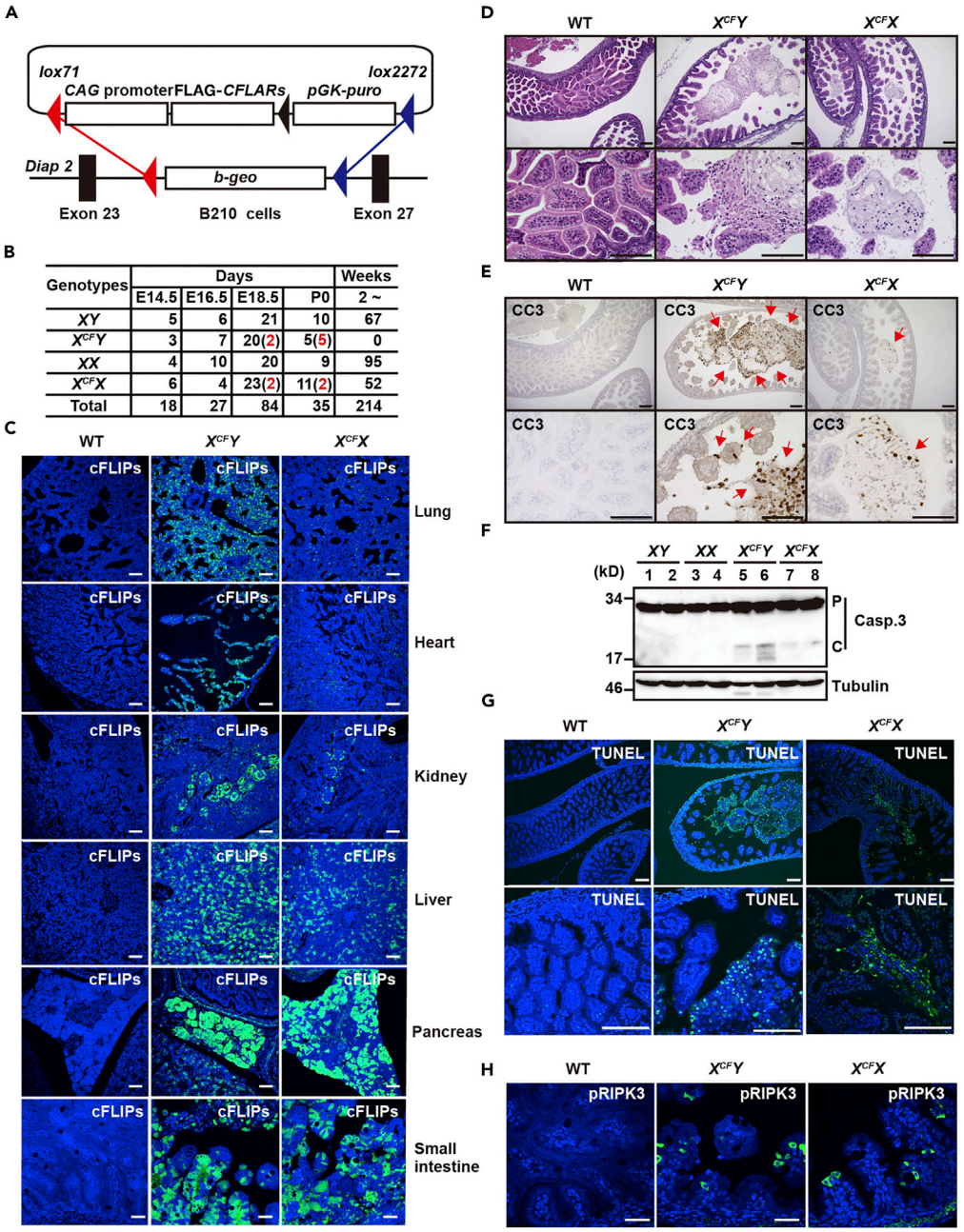

Genotypes	Days				Weeks
	E14.5	E16.5	E18.5	P0	2 ~
XY	5	6	21	10	67
$X^{CF}Y$	3	7	20(2)	5(5)	0
XX	4	10	20	9	95
$X^{CF}X$	6	4	23(2)	11(2)	52
Total	18	27	84	35	214

Figure 1. *CFLARs* Tg Mice Die Perinatally

(A) Diagram of a vector for *CFLARs* Tg mice and genomic organization of the *Diap2* locus of B210 cells.

(B) $X^{CF}Y$ mice die perinatally. After timed mating, mice were sacrificed at the indicated days after coitus, and the genotypes of embryos were determined by PCR. Numbers in parentheses written in red characters indicate dead pups at the sacrifice. The genotypes of 2- to 4-week-old mice were determined by PCR.

(C) Tissue sections from mice of the indicated genotypes at E18.5 were stained with anti-cFLIP antibody (n = 3–5 mice per each genotype). The tyramid signal amplification (TSA) method was used to enhance cFLIPs-positive signals. Scale bars, 50 μm. Notably, anti-cFLIP antibody recognized exogenously expressed human cFLIPs, but endogenous murine cFLIP at least under our experimental conditions.

(D) H&E-stained small intestinal sections of mice of the indicated genotypes at E18.5 (n = 10 mice per each genotype). Scale bars, 100 μm.

(E, G, and H) Small intestinal tissue sections of mice of the indicated genotypes at E18.5 were stained with anti-cleaved caspase 3 (CC3) (E) or pRIPK3 (H) antibodies, or subjected to TUNEL staining (G) (n = 3–4 mice per each genotype). Scale bars, 100 μm. Red arrows indicate CC3+ IECs.

Figure 1. *Continued*

(F) Tissue extracts of the SI of mice of the indicated genotypes at E18.5 were immunoblotted with the indicated antibodies (n = 2 per genotype). Each number indicates an individual mouse. P and C indicate the proform and cleaved form caspase 3, respectively. Results are representative of two independent experiments. See also Figures S1 and S2.

We next tested whether IECs of *CFLARs* Tg mice died by necroptosis. As phosphorylation of RIPK3 (pRIPK3) is a hallmark of cells dying by necroptosis, antibodies that recognize pRIPK3 have been used to detect necroptotic cells by IHC (Webster et al., 2018). We found that small numbers of pRIPK3-positive cells were detected in the SI and other tissues of *CFLARs* Tg mice (Figures 1H and S1B), suggesting these cells died by necroptosis. In contrast, apoptotic cells were not detected in tissues other than SI (Figure S1C). Together, these results suggest that IECs mainly died by apoptosis rather than necroptosis in *CFLARs* Tg mice at E18.5.

We established two lines of *CFLARs* Tg mice, designated C9 and C28, and verified the expression of cFLIPs in various tissues of adult $X^{CF}X$ mice by western blot (Figure S1D). We found that a few CC3-positive cells were still observed in the SI, but not in the colon of adult $X^{CF}X$ mice (Figures S1E–S1G). As the phenotypes of C9 and C28 mice were identical, we mainly analyzed a C28 line for further experiments.

To exclude the possibility that the phenotype of *CFLARs* Tg mice might come from inactivation of *Diap2* gene, we also generated another Tg mice line, in which *Cre-ERT2* was integrated into the same locus on the X chromosome, designated *Cre-ERT2* Tg mice (Figure S2A). *Cre-ERT2* Tg mice were born at the expected Mendelian ratios (Figure S2B) and did not show any abnormality of the SI and colon (Figures S2C–S2E). These results indicate that the phenotype of *CFLARs* Tg mice is not caused by inactivation of *Diap2* gene, but the expression of *CFLARs* gene.

A Few IECs Already Undergo Necroptosis in the SI of *CFLARs* Tg Mice at E17.5

To investigate an interplay between apoptosis and necroptosis, we analyzed histology of IECs at an earlier time point E17.5. IECs of *CFLARs* Tg mice appeared to be normal at E17.5 compared with those at E18.5 (Figure 2A). Notably, pRIPK3-positive cells were detected in the SI of *CFLARs* Tg mice similarly to E18.5 (Figure 2B), whereas very few IECs were positive for CC3 staining (Figure 2C). TEM analysis revealed that some IECs exhibited a drastic decrease in electron densities of the cytoplasm with the dilatation of the endoplasmic reticulum and mitochondria in *CFLARs* Tg mice, suggesting that these IECs died by necroptosis (Figure 2D). In sharp contrast, a few IECs were detached from villi and exhibited chromatin condensation, a hallmark of apoptosis (Figure 2D). To quantify the relative populations of necroptotic and apoptotic cells, we calculated $TUNEL^+$ and $CC3^+$ cells, respectively. TUNEL staining recognizes both necroptotic and apoptotic cells. Numbers of $TUNEL^+$ cells were higher than those of $CC3^+$ cells in the SI of *CFLARs* Tg mice (Figures 2C, 2E, and 2F), thus IECs already started to die by necroptosis, and to a lesser extent, by apoptosis at E17.5.

Deletion of *Ripk3* Gene Partially Rescues Embryonic Lethality of *CFLARs* Tg Mice

To investigate the causal relationship between necroptosis and apoptosis, we crossed *CFLARs* Tg mice with *Ripk3*−/− mice (Newton et al., 2004). Deletion of *Ripk3* partially rescued embryonic lethality of $X^{CF}Y$ mice and blocked the destruction of the villous structure in the SI of both $X^{CF}Y$ and $X^{CF}X$ mice (Figures 3A and 3B). As expected, pRIPK3-positive IECs disappeared in the SI of $X^{CF}Y$;*Ripk3*−/− and $X^{CF}X$;*Ripk3*−/− mice at E18.5 (Figure 3C). More importantly, CC3-positive IECs also disappeared in the SI of $X^{CF}Y$;*Ripk3*−/− and $X^{CF}X$;*Ripk3*−/− mice at E18.5 (Figure 3D). TEM analysis confirmed that apoptosis and necroptosis of IECs disappeared in the SI of $X^{CF}Y$;*Ripk3*−/− mice (Figure S3A). Survived $X^{CF}Y$;*Ripk3*−/− mice appeared to be healthy (Figures S3B–S3D). cFLIPs protein was ubiquitously expressed in various tissues of surviving $X^{CF}Y$;*Ripk3*−/− mice, and their expression levels were higher than those of $X^{CF}X$ mice on a *Ripk3*−/− or *Ripk3*+/− background (Figure S3E). Necroptosis of IECs occurs in IEC-specific *Fadd*- or *Caspase 8*-deficient mice (Gunther et al., 2011; Welz et al., 2011), suggesting that necroptosis independently occurs in the absence of apoptosis. However, it is unclear whether necroptosis promotes or suppresses apoptosis *in vivo*. Taken that deletion of *Ripk3* blocked necroptosis and apoptosis, necroptosis might promote apoptosis of IECs of *CFLARs* Tg mice *in vivo*.

Consistent with these results, TNF and zVAD-fmk (TNF/zVAD)-induced necroptosis were enhanced in murine embryonic fibroblasts (MEFs) derived from $X^{CF}Y$;*Ripk3*+/− mice compared with *Ripk3*+/− mice, and TNF/zVAD-induced necroptosis was abolished in MEFs from $X^{CF}Y$ mice on a *Ripk3*-deficient background (Figure 3E).

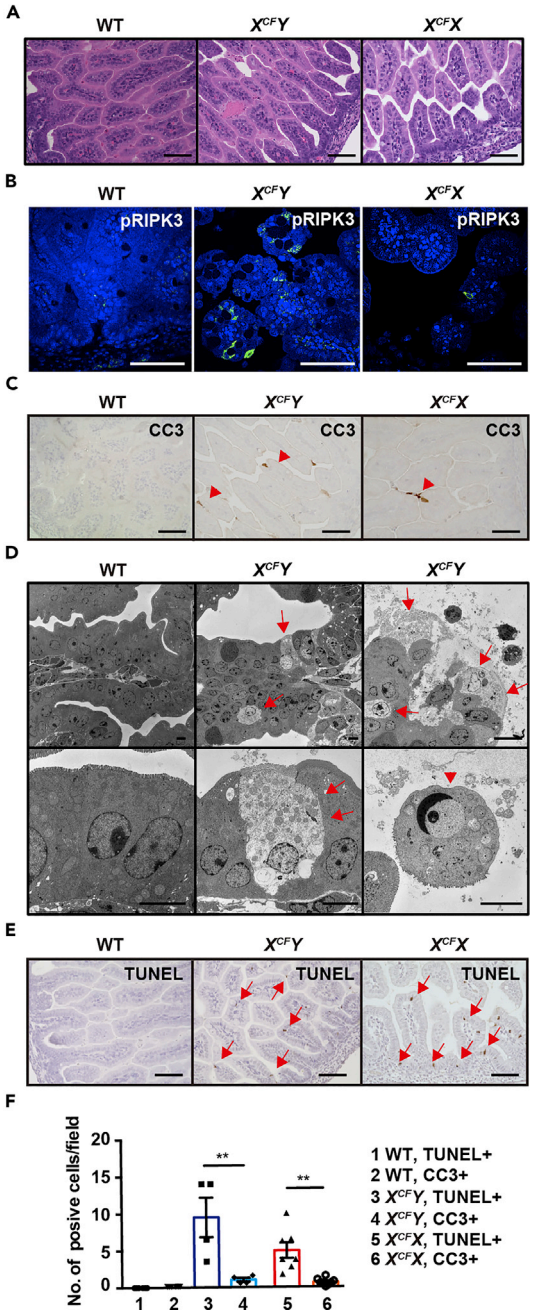

Figure 2. A Few IECs Already Undergo Necroptosis in the SI of *CFLAR*s Tg Mice at E17.5

(A–C and E) Small intestinal sections of mice of the indicated genotypes at E17.5 were stained with H&E (A), anti-pRIPK3 (B), or anti-CC3 (C) antibodies, or subjected to TUNEL staining (E). Red arrowheads and arrows indicate CC3+ (C) and TUNEL+ cells (E), respectively. Results are representative of four independent experiments (n = 4 mice per each genotype). Scale bars, 100 μm.

(D) Tissue sections described as in (A) were analyzed by TEM (n = 4 mice per each genotype). Red arrows and arrowheads indicate cells showing necroptotic and apoptotic morphology, respectively. Scale bars, 5 μm.

(F) Numbers of CC3-positive and TUNEL-positive cells were counted in randomly selected fields and are expressed as numbers of positive cells per field. Results are mean ± SEM (n = 4–7 mice per genotype). Statistical significance was determined by two-tailed unpaired Student's t test. **p < 0.01; ns, not significant.

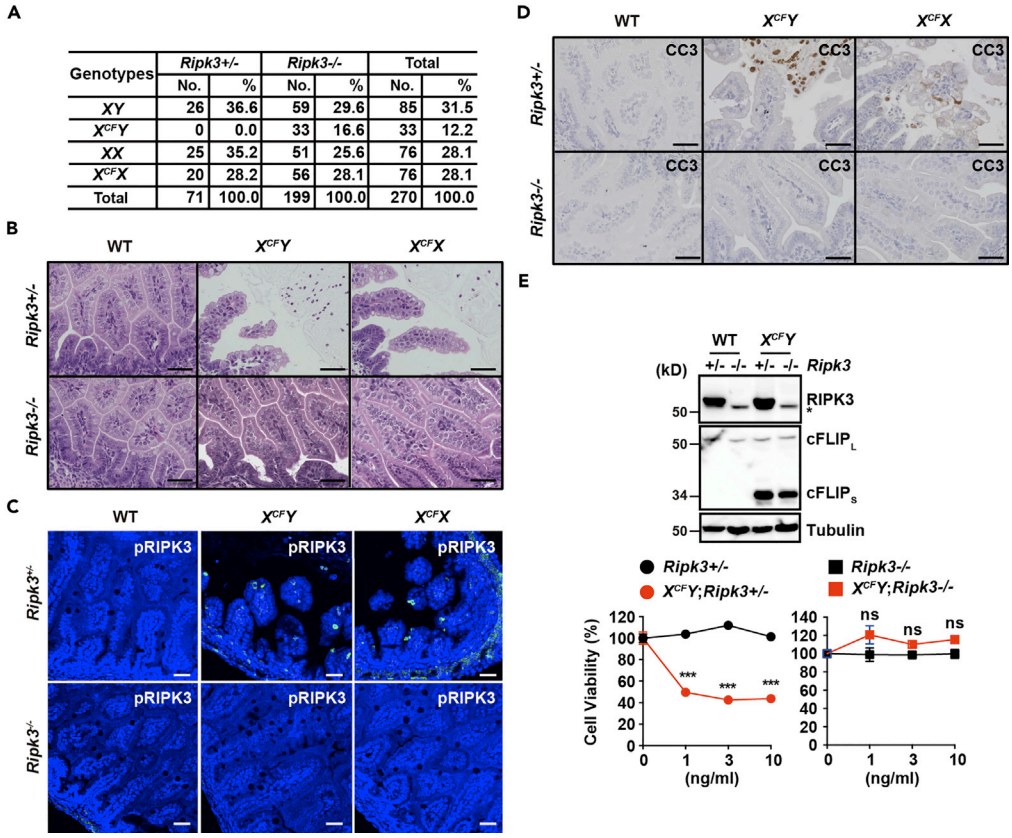

Figure 3. Deletion of *Ripk3* Partially Rescues Embryonic Lethality of *CFLARs* Tg Mice

(A) The progeny of crossing male *Ripk3*−/− mice with $X^{CF}X$;*Ripk3*−/− or $X^{CF}X$;*Ripk3*+/− mice. The genotypes of 3- to 4-week-old mice were determined by PCR.

(B) Small intestinal sections of mice of the indicated genotypes at E18.5 were stained with H&E (n = 4 mice per each genotype). Scale bars, 100 μm.

(C and D) Intestinal sections of mice of the indicated genotypes at E18.5 were stained with anti-pRIPK3 (C) or anti-CC3 (D) antibodies (n = 3–4 mice per each genotype). Scale bars, 100 μm.

(E) Primary MEFs were prepared from mice of the indicated genotypes at E14.5 and the expression of each protein was verified by western blot with the indicated antibodies. MEFs were stimulated with the indicated concentrations of TNF and zVAD-fmk (20 μM) for 7 h. Cell viability was determined by water soluble tetrazolium monosodium salt (WST) assay. Results are mean ± SD of triplicate samples and representative of three independent experiments. Statistical significance was determined by the two-tailed unpaired Student's t test. ***$p < 0.001$; ns, not significant. See also Figure S3.

Deletion of *Mlkl* or Inactivation of RIPK1 Kinase Activity Partially Rescue Embryonic Lethality of *CFLARs* Tg Mice

Although RIPK3 is essential for necroptosis, several studies have shown that RIPK3 promotes apoptosis and also inflammation under certain conditions (Mandal et al., 2014; Newton et al., 2014). Taken that MLKL solely promotes necroptosis (Murphy et al., 2013; Wu et al., 2013), we crossed *CFLARs* Tg mice with *Mlkl*−/− mice (Dannappel et al., 2014). Consistent with deletion of *Ripk3*, deletion of *Mlkl* partially rescued the lethal phenotype of $X^{CF}Y$ mice and blocked the disruption of the villous structure of the SI of $X^{CF}Y$ mice (Figures 4A and 4B). Moreover, CC3-positive, but not pRIPK3-positive, IECs disappeared in the SI of $X^{CF}Y$;*Mlkl*−/− mice (Figures 4C and 4D). These results suggest that MLKL-dependent necroptosis subsequently triggers apoptosis of IECs *in vivo*.

RIPK1 kinase activity is required for formation of the complex IIb that is composed of FADD, caspase 8, RIPK1, and RIPK3 and induces apoptosis or necroptosis in a context-dependent manner (Feoktistova et al., 2011; Tenev et al., 2011). Crossing of *CFLARs* Tg mice with mice expressing a kinase-inactive mutant of *Ripk1* (*Ripk1*$^{DN/DN}$) (Polykratis et al., 2014) more efficiently rescued lethal phenotype of *CFLARs*

A

Genotypes	No.	%
XY;Mlkl-/-	55	32.9
$X^{CF}Y$*;Mlkl-/-*	11	6.6
XX;Mlkl-/-	52	31.1
$X^{CF}X$*;Mlkl-/-*	49	29.3
Total	98	100

E

Genotypes	No.	%
XY;Ripk1$^{DN/DN}$	34	24.6
$X^{CF}Y$*;Ripk1*$^{DN/DN}$	23	16.7
XX;Ripk1$^{DN/DN}$	36	26.1
$X^{CF}X$*;Ripk1*$^{DN/DN}$	45	32.6
Total	138	100

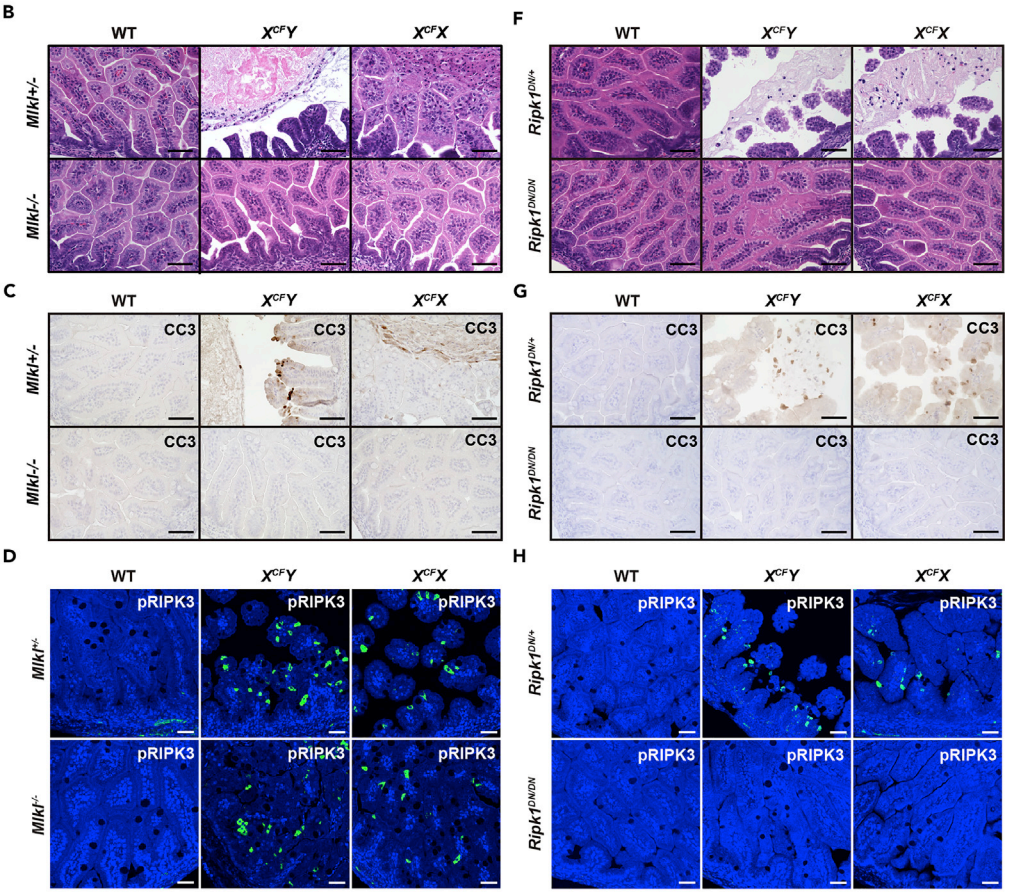

I

Genotypes	No.	%
XY;Tnfrsf1a-/-	53	50
$X^{CF}Y$*;Tnfrsf1a-/-*	0	0
XX;Tnfrsf1a-/-	37	34.9
$X^{CF}X$*;Tnfrsf1a-/-*	16	15.1
Total	106	100

Figure 4. Deletion of *Mlkl* or Inactivation of RIPK1 Kinase Activity Partially Rescues Embryonic Lethality of *CFLARs* Tg Mice

(A, E, and I) The progeny of crossing wild-type male mice with $X^{CF}X$ mice on an *Mlkl−/−* (A), *Ripk1*$^{DN/DN}$ (E), or *Tnfrsf1a−/−* (I) background. The genotypes of 3- to 4-week-old mice were determined by PCR.

(B and F) Small intestinal sections of mice of the indicated genotypes at E18.5 were stained with H&E (n = 3–4 mice per each group).

(C, D, G, and H) Small intestinal sections of mice of the indicated genotypes at E18.5 were stained with anti-CC3 (C and G) or anti-pRIPK3 (D and H) antibodies (n = 3–4 mice per each genotype).

Scale bars, 100 μm.

Tg mice compared with *Mlkl−/−* mice by preventing both necroptosis and apoptosis (Figures 4E–4H). Unexpectedly, *Tnfrsf1a* deficiency (Pfeffer et al., 1993) could not rescue lethal phenotype of $X^{CF}Y$ mice (Figure 4I), suggesting that the cFLIPs promote the RIPK3-MLKL-dependent necroptotic pathway in IECs of *CFLARs* Tg mice in a TNFR1-independent manner.

The Expressions of Reg3β and Reg3γ Are Elevated in the SI of *CFLARs* Tg Mice

To further investigate the consequences of cFLIPs-dependent cell death *in vivo*, we performed genome-wide transcriptome analysis of the SI of wild-type and *CFLARs* Tg mice at E18.5. We found that genes associated with cytokine responses, inflammatory responses, innate immune responses, and host defense responses were enriched in the SI of *CFLARs* Tg mice compared with wild-type mice (Figures S4A–S4C; Table S1). We focused on *Regenerating gene* (*Reg*)*3b* and *Reg3g*. Reg3β and Reg3γ are produced by IECs and act as antimicrobial proteins (Vaishnava et al., 2011). Notably, the expressions of *Reg3b* and *Reg3g* are tightly regulated at the developmental stages: both *Reg3b* and *Reg3g* are not expressed in the SI of wild-type fetus, but their expression is gradually increased in the SI after birth possibly due to colonization with commensal bacteria (Matsumoto et al., 2012). We confirmed that the expression of *Reg3b* and *Reg3g* was undetectable in the SI of wild-type mice, but elevated in the SI of *CFLARs* Tg mice at E18.5 by qPCR, IHC, and western blot (Figures S5A–S5C; Table S2).

We next investigated the mechanism underlying the elevation of *Reg3b* and *Reg3g* in the SI of adult mice. The expression of *Reg3b* and *Reg3g* in the SI of adult mice was abolished in *Il22*−/− (Zheng et al., 2008) or *Rorc-gfp/gfp* (Eberl et al., 2004), but not in *Rag2*−/− (Hao and Rajewsky, 2001) mice (Figure S5D). However, *Rorc* is essential for the development of ILC3s and T_H17 cells, and the expression of *Il22* was abolished in the SI of *Rorc-gfp/gfp*, but not in *Rag2*−/− mice (Figure S5E). These results suggest that IL-22 produced by RORγt$^+$ ILC3s, but not T_H17 cells, is essential for the expression of *Reg3b* and *Reg3g* in the SI of adult mice. Thus we surmised that RORγt$^+$ ILC3s might be activated in response to cell death of IECs of *CFLARs* Tg mice at the prenatal stage.

ILC3s Accumulate in the SI of *CFLARs* Tg Mice

Although ILC3s play a crucial role in maintaining tissue homeostasis of the intestine (Ouyang and Valdez, 2008; Parks et al., 2015), activation of ILC3s promotes intestinal tissue injury under certain conditions (Bauche et al., 2018; Eken et al., 2014). ILC3s are aberrantly activated in the SI of mice lacking CD4$^+$ T cells or young mice wherein acquired immunity is not fully maturated (Mao et al., 2018). As expected, the expression of *Foxp3*, a hallmark of Treg cells, was very low in the SI of either wild-type or *CFLARs* Tg mice at E18.5 compared with that of adult mice (Figure S6A). To test whether ILC3s contribute to the development of ileitis at preterm mice, we first crossed *Rorc-gfp* reporter mice with *CFLARs* Tg mice. As the expression of the green fluorescent protein (GFP) is under the control of endogenous promoter of *Rorc* in *Rorc-gfp* reporter mice, RORγt$^+$ cells that contain both T_H17 cells and ILC3s are recognized as GFP$^+$ cells by flow cytometry or IHC. We found that large numbers of CD11b$^+$Ly-6G$^+$ neutrophils infiltrated in the SI of *CFLARs* Tg mice at E18.5 (Figures 5A and 5B). CCR6$^+$ ILC3s are recruited to the SI via its ligand CCL20 that is produced by IECs (Esplugues et al., 2011). Although total numbers of GFP (RORγt)$^+$ ILC3s were not increased in *CFLARs* Tg mice compared with wild-type mice (Figures 5A and 5B), RORγt$^+$ cells were recruited to the SI along with an increase in the expression of CCL20 and an appearance of apoptotic cells (Figure 5C).

To determine whether apoptotic cells were responsible for accumulation of RORγt$^+$ cells, we tested whether RORγt$^+$ cells accumulated in the SI at E17.5. Although we hardly detected or only detected very few apoptotic cells in the SI of *CFLARs* Tg mice (Figures 2C and 5D), a number of RORγt$^+$ cells were already recruited to the SI along with an increase in the expression of CCL20 (Figure 5D). As we hardly detected CD3$^+$ T cells in the SI of *CFLARs* Tg mice at E17.5 and E18.5 by IHC (data not shown), accumulated RORγt$^+$ cells were ILC3s, but not T_H17 cells. Accumulation of neutrophils appeared to delay compared with that of ILC3s (Figures 5C and 5D), suggesting that neutrophils might not be primarily responsible for apoptosis induction, but accumulated in response to apoptotic cells. The expression of CCL20 was elevated in the SI of *CFLARs* Tg mice along with an appearance of necroptotic cells, whereas its expression was abrogated in *CFLARs* Tg mice on a *Ripk3*−/− or *Mlkl*−/− background (Figure 5E). Notably, although only small numbers of IECs underwent necroptosis (Figure 1H), CCL20 was ubiquitously expressed in all IECs (Figure 5C). Inflammatory cytokines such as TNF and IL-1β have been shown to induce CCL20 production by IECs (Kwon et al., 2002), and macrophages and dendritic cells might produce these cytokines in response to danger-associated molecular pattern (DAMP)s released from necroptotic IECs. Taken that the expression of *Il1b* was elevated in the SI of *CFLARs* Tg mice (Figure S6C), IL-1β might be responsible for the production of CCL20 by IECs. Consistently, the expression of both *Il1b* and *Ccl20*, but not *Il22*, was significantly elevated in the SI of *CFLARs* Tg mice at E17.5 (Figure S6D), suggesting an intimate cross talk between the expression of *Il1b* and *Ccl20*. Moreover, IL-1β and IL-23 have been shown to activate ILC3s (Manta et al., 2013; Mortha et al., 2014). Together, IL-1β might be responsible for CCL20 production by IECs and activation of ILC3s.

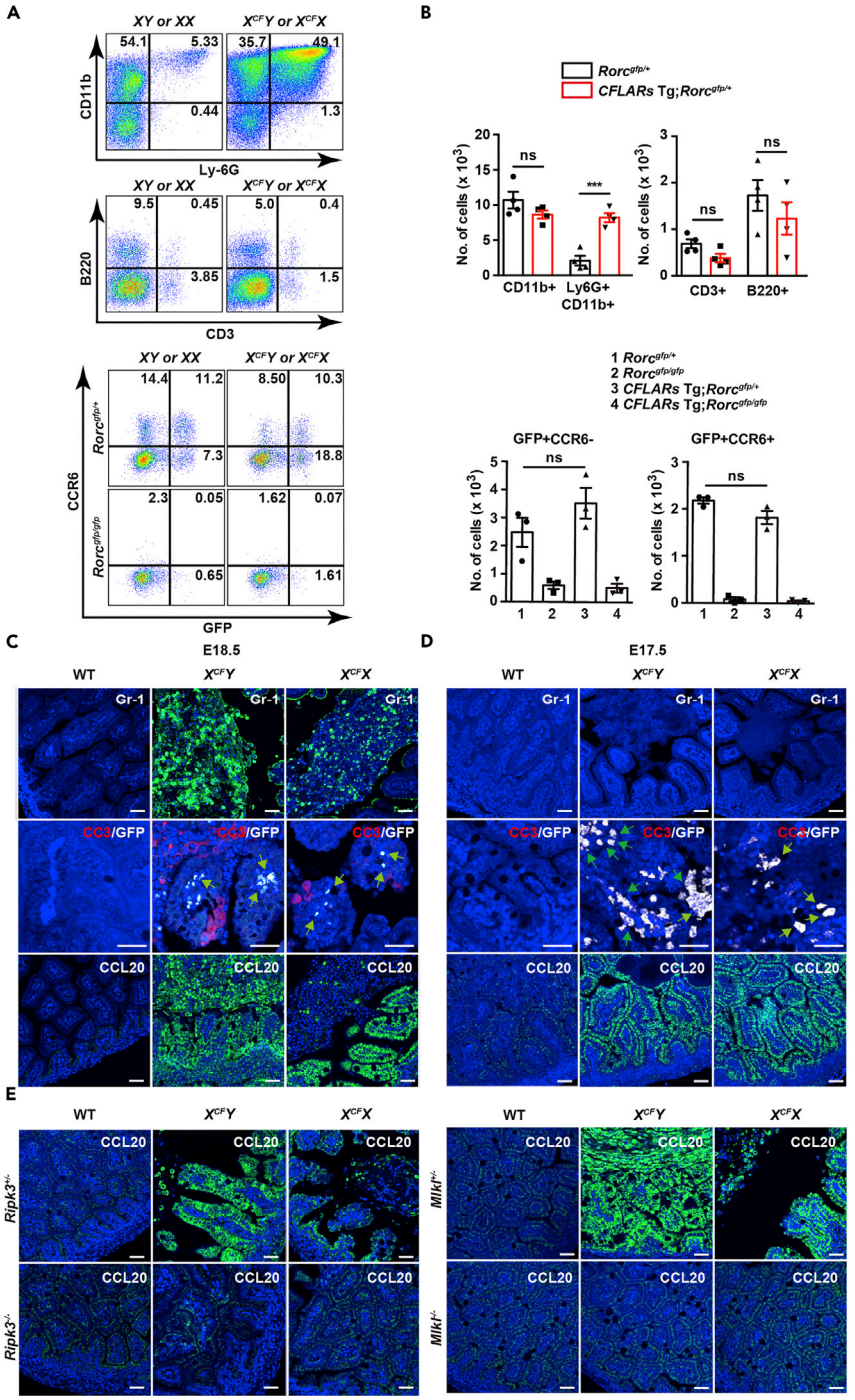

Figure 5. ILC3s Accumulate in the SI of *CFLARs* Tg Mice

(A) Percentages of neutrophils, but not T cells, B cells, or RORγt$^+$ cells are increased in the SI of *CFLARs* Tg mice at E18.5 compared with WT mice. Cells were prepared from the SI of WT or *CFLARs* Tg mice at E18.5, and pooled samples (approximately 3–4 fetal SI per each genotype) were stained with the indicated antibodies and analyzed by flow cytometry. Results are representative of four independent experiments.

(B) Cells were prepared as in (A); absolute cell numbers of the indicated populations were calculated and are expressed as mean ± SEM of four independent experiments. Statistical significance was determined by the two-tailed unpaired Student's t test. ***$p < 0.001$; ns, not significant.

Figure 5. *Continued*

(C and D) Small intestinal sections of mice of WT, $X^{CF}Y$;*Rorc-gfp/+*, and $X^{CF}X$;*Rorc-gfp/+* mice at E18.5 (C) and E17.5 (D) were stained with anti-Gr-1, combination of anti-GFP (to detect RORγt$^+$ cells) (white) and anti-CC3 (red), or anti-CCL20 antibodies (n = 3 mice per each genotype). Green arrows indicate RORγt$^+$ cells. Scale bars, 100 μm.

(E) Small intestinal sections of mice of the indicated genotypes were stained with anti-CCL20 (n = 3 mice per each genotype). Scale bars, 100 μm.

See also Figures S4–S6, and Table S1.

Deletion of *Rorc* or *Il22* Partially Rescues Embryonic Lethality of *CFLARs* Tg Mice

We next tested whether ILC3s might contribute to the development of ileitis in *CFLARs* Tg mice. Deletion of *Rorc* partially rescued embryonic lethality of $X^{CF}Y$ mice and blocked the destruction of villi structure of the SI of *CFLARs* Tg mice (Figures 6A and 6B). A large numbers of neutrophils and CC3-positive IECs were detected in the SI of $X^{CF}Y$;*Rorc-gfp/+* mice, whereas infiltration of these cells almost completely disappeared in the SI of $X^{CF}Y$;*Rorc-gfp/gfp* mice (Figures 6C and 6D). CXCL2 is a chemokine that recruits neutrophils (Kobayashi, 2008). Consistently, the expressions of *Reg3b, Reg3g, Il22, Cxcl2,* and *Ccl20* were downregulated in the SI of *CFLARs* Tg mice on a *Rorc-gfp/gfp* background (Figure S7A). pRIPK3-positive IECs were still detected in the SI of *CFLARs* Tg mice on a *Rorc-gfp/gfp* background (Figure 6E), further substantiating that activation of RORγt$^+$ ILC3s is a downstream event of necroptosis of IECs of *CFLARs* Tg mice.

Previous studies have reported that IL-22 has anti-colitogenic or colitogenic functions in a context-dependent manner (Eken et al., 2014; Ouyang and Valdez, 2008). To determine the contribution of IL-22 to the development of ileitis in *CFLARs* Tg mice, we finally crossed *CFLARs* Tg mice with *Il22*−/− mice. Deletion of *Il22* partially rescued embryonic lethality and prevented the development of ileitis in *CFLARs* Tg mice (Figures 6F–6H). Notably, CC3-positive cells completely disappeared in the SI of *CFLARs* Tg;*Il22*−/− mice (Figure 6I), but pRIPK3-positive cells were still detected (Figure 6J). Moreover, the expression of *Reg3b, Reg3g, Cxcl2,* and *Ccl20* was downregulated in the SI of *CFLARs* Tg;*Il22*−/− mice (Figure S7A). Thus IL-22 contributes, at least in part, to intestinal injury at perinatal stages. Moreover, deletion of *Ripk3, Mlkl,* or kinase activity of RIPK1 downregulated the expression of these genes (Figure S7A), suggesting that the execution of necroptosis finally converged on recruitment and activation of ILC3s and IL-22 production.

We finally investigated the mechanism underlying IL-22-dependent tissue injury. We found that the expression of reactive oxygen species (ROS)-producing enzyme, *Duox2* and its regulatory subunit, *Duoxa2*, were significantly elevated in the SI of *CFLARs* Tg mice (Figure S7B). *DUOX2* is upregulated in patients with inflammatory bowel disease (IBD) before the onset of inflammation and is a marker of perturbed mucosal homeostasis in patients with early-stage IBD (Grasberger et al., 2015). Taken that IL-22 induces the expression of *Duox2* of IECs (Grasberger et al., 2015), it is reasonable to speculate that ILC3s might induce ROS-dependent apoptosis of IECs through the IL-22-Duox2 pathway. Together, these results indicate that a positive feedforward loop between cFLIPs-dependent necroptosis (Figure 7A) and ILC3-dependent apoptosis might critically contribute to the development of lethal ileitis in neonatal mice (Figure 7B).

DISCUSSION

In the present study, we generated transgenic mice expressing human *CFLARs* on the X chromosome and investigated cellular responses triggered by necroptosis *in vivo*. As expected, all male *CFLARs* Tg mice died *in utero*, but female *CFLARs* Tg mice survived due to X chromosome inactivation. Thus the expression of cell-death-promoting gene on the X chromosome might be one of the strategies to evaluate cellular responses triggered by cell death *in vivo*. Although cFLIPs blocks caspase-dependent apoptosis but promotes necroptosis *in vitro* (Feoktistova et al., 2011; Oberst et al., 2011), IECs died by necroptosis and apoptosis in *CFLARs* Tg mice. Deletion of *Ripk3* or *Mlkl*, or inhibition of kinase activity of RIPK1, partially prevented embryonic lethality of *CFLARs* Tg mice by suppressing both apoptosis and necroptosis of IECs. We finally showed that ILC3s induced apoptosis of IECs in an IL-22-dependent manner, culminating in the development of lethal ileitis in *CFLARs* Tg mice.

In sharp contrast to *in vitro* studies including ours (Feoktistova et al., 2011; Oberst et al., 2011; Shindo et al., 2013), overexpression of cFLIPs *in vivo* resulted in both apoptosis and necroptosis of IECs in mice. Taken

A

Genotypes	*Rorc*$^{gfp/+}$		*Rorc*$^{gfp/gfp}$		Total	
	No	%	No	%	No	%
XY	61	33.0	112	31.8	173	32.2
$X^{CF}Y$	2	1.1	43	12.2	45	8.4
XX	71	38.4	99	28.1	170	31.7
$X^{CF}X$	51	27.6	98	27.8	149	27.7
Total	185	100.0	352	100.0	537	100.0

F

Genotypes	*Il22*$^{+/-}$		*Il22*$^{-/-}$		Total	
	No	%	No	%	No	%
XY	26	34.7	30	23.3	56	27.5
$X^{CF}Y$	0	0.0	18	14.0	18	8.8
XX	28	37.3	51	39.5	79	38.7
$X^{CF}X$	21	28.0	30	23.3	51	25.0
Total	75	100.0	129	100.0	204	100.0

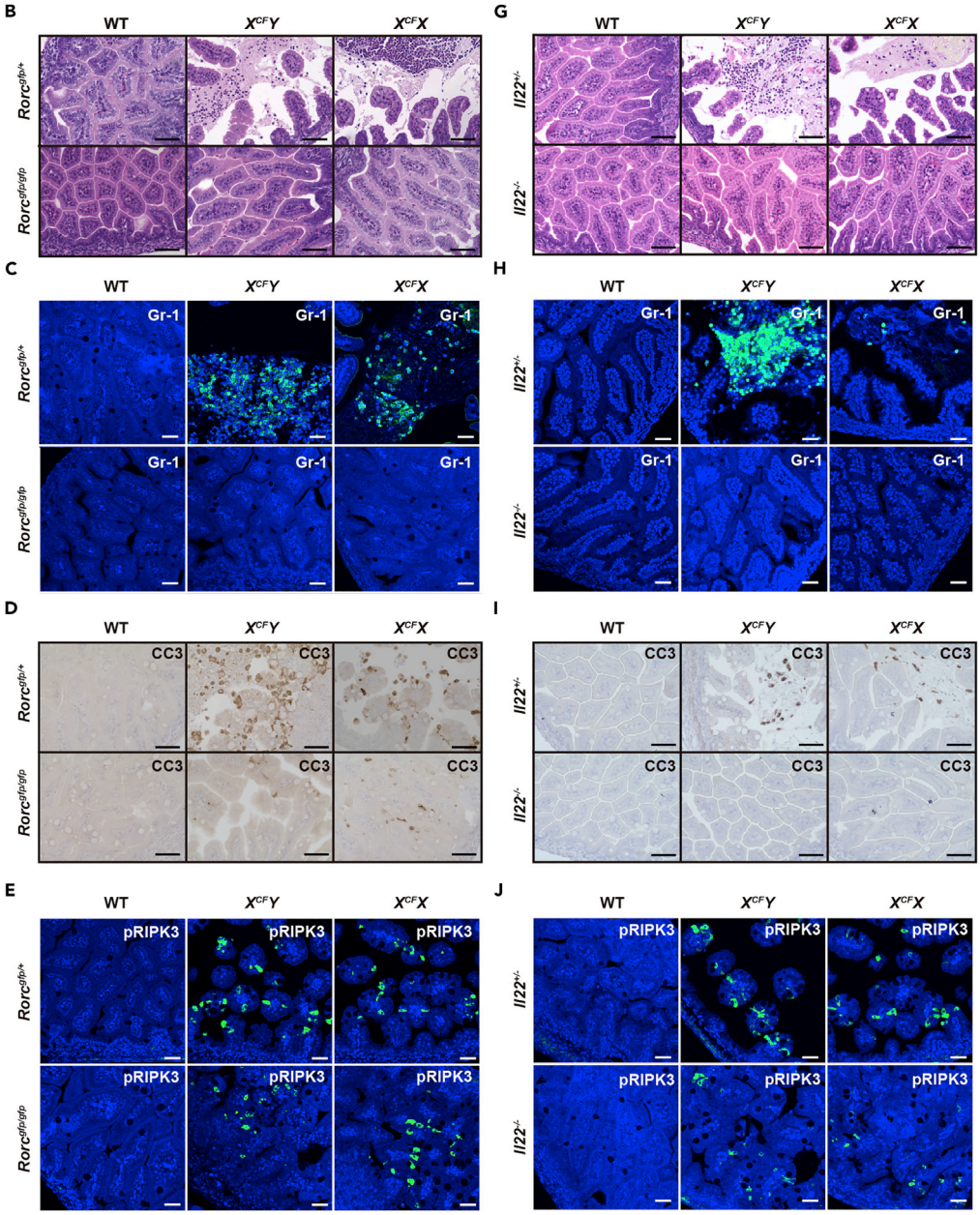

Figure 6. Deletion of *Rorc* or *Il22* Partially Rescues Embryonic Lethality of *CFLARs* Tg Mice

(A and F) The progeny of crossing male *Rorc-gfp/gfp* (A) or *Il22−/−* (F) mice with $X^{CF}X$ mice. The genotypes of 3- to 4-week-old mice were determined by PCR.

(B–E and G–J) Intestinal sections of mice of the indicated genotypes at E18.5 were stained with H&E (B and G), anti-Gr-1 (C and H), anti-CC3 (D and I), or anti-pRIPK3 (E and J) antibodies (n = 3–4 mice per group).

Scale bars, 100 μm. See also Figure S7.

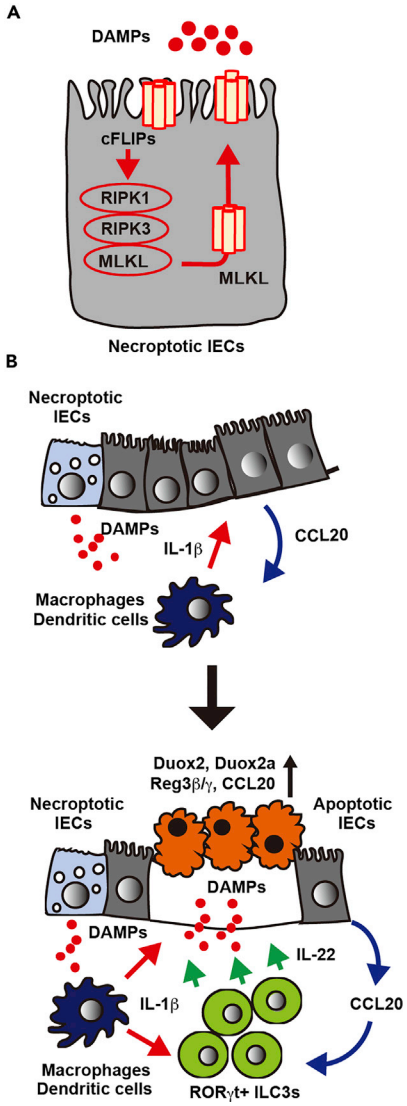

Figure 7. A Model for cFLIPs-Dependent Lethal Ileitis

(A) The complex IIb spontaneously forms in IECs overexpressing cFLIPs. As cFLIPs blocks activation of caspase 8, the complex IIb evolves into the necrosome, resulting in oligomerization of MLKL and subsequent membrane permeabilization.

(B) Necroptotic cells of IECs release DAMPs that subsequently activate nearby macrophages or dendritic cells, resulting in IL-1β production. In addition to the release of DAMPs, IECs in response to IL-1β produce CCL20 that recruits CCR6-positive ILC3s into IECs. Recruited IEC3s are activated by IL-1β and release IL-22 that acts on IECs, resulting in upregulation of *Reg3b*, *Reg3g*, *Duox2*, and *Duoxa2*. Importantly, aberrantly activated ILC3s induce apoptosis of IECs possibly through upregulation of several ROS-producing enzymes. Apoptotic IECs might enhance inflammation and further activate ILC3s. Thus blockade of the necroptotic pathway and depletion of ILC3s or *Il22* suppress lethal ileitis.

that cFLIPs inhibits death receptor-induced apoptosis *in vitro* (Feoktistova et al., 2011; Oberst et al., 2011), and deletion of *Tnfrsf1a* did not attenuate embryonic lethality of *CFLARs* Tg mice, death receptor-induced caspase 8-dependent pathway is not primarily responsible for the execution of apoptosis of IECs of *CFLARs* Tg mice. Notably, the expression of *Duox2* and its regulatory subunit, *Duoxa2,* were elevated in the SI of *CFLARs* Tg mice compared with control mice. Taken that oxidative stress has been shown to induce apoptosis under certain conditions (Circu and Aw, 2010), ROS-dependent activation of effector caspases might promote apoptosis of IECs in *CFLARs* Tg mice.

Histological analysis revealed that severe tissue injury was restricted to the SI of *CFLARs* Tg mice. We found that ILC3s were only detected in the SI and the liver, but not other tissues. Intriguingly, ILC3s were detected even in the liver of wild-type mice, suggesting that these cells were resident ILC3s, but not infiltrated ILC3s in response to certain stimuli observed in the SI of *CFLARs* Tg mice. These results suggest that cFLIPs-dependent tissue injury is correlated with infiltration of ILC3s in response to necroptotic cells. Although male *CFLARs* Tg;*Ripk3*−/− mice did not show any abnormality of the SI at E18.5, deletion of *Ripk3* did not completely rescue embryonic lethality of *CFLARs* Tg mice. This suggests that the cause of lethality of *CFLARs* Tg;*Ripk3*−/− mice was not ileitis. A recent study showed that white blood cells are markedly increased in the peripheral blood of *Ripk1*−/− mice and *Ripk1*−/− hematopoietic cells fail to engraft efficiently in lethally irradiated wild-type (WT) mice (Peltzer et al., 2018; Rickard et al., 2014). Thus bone marrow (BM) failure might induce embryonic lethality of *CFLARs* Tg;*Ripk3*−/− mice when intestinal tissue injury was attenuated. Moreover, percentages of survived $X^{CF}Y$ mice on an *Mlkl*−/− background were lower than those on *Ripk3*−/− or $Ripk1^{DN/DN}$ background. Notably, RIPK1 kinase activity and RIPK3 are involved in inflammation and apoptosis under certain conditions (Pasparakis and Vandenabeele, 2015), suggesting that the MLKL-independent pathways also contribute to embryonic lethality of *CFLARs* Tg mice. Further study will be required to address these issues.

Although approximately 10% of $X^{CF}X$ mice died perinatally, other $X^{CF}X$ mice survived until adulthood. One might surmise that IECs susceptible to cFLIPs-induced cell death have been largely eliminated during the development *in utero* or soon after birth. Therefore few IECs might be positive for CC3 staining. On the other hand, Treg cells are very few in the SI during embryonic stages and then gradually expand along with colonization of commensal bacteria (Honda and Littman, 2016). We found that the expression of *Foxp3* in the SI of either wild-type or *CFLARs* Tg mice at E18.5 was very low compared with that of adult mice. Intriguingly, $LAG3^{+}$ regulatory T cells restrain IL-23- and IL-1β-producing macrophages, thereby suppressing activation of ILC3s and the development of intestinal injury (Bauche et al., 2018). Aberrant activation of ILC3 by IL-23 has been shown to drive IL-22-dependent intestinal inflammation (Buonocore et al., 2010). Moreover, *Il23* transgenic mice spontaneously develop severe intestinal inflammation along with accumulation of ILC3s and neutrophils in the SI at neonatal stages (Chen et al., 2015). The development of intestinal inflammation of *Il23* Tg mice is blocked when ILC3s are depleted, or mice are treated with antibiotics, suggesting that commensal bacteria-dependent production of IL-23 might contribute to the development of severe intestinal inflammation at the neonatal stage. Given that numbers of maturated Treg cells were very few in *CFLARs* Tg at E18.5, Treg cells did not attenuate ILC3s-dependent ileitis in neonatal *CFLARs* Tg mice. In contrast, ileitis might be attenuated by Treg cells in adult $X^{CF}X$ mice. Together, these studies have revealed the critical contribution of ILC3s to the development of severe ileitis in mice at prenatal stages.

Previous studies have shown that germline deletion of *Caspase 8* or *Fadd* in mice promotes necroptosis *in utero*, resulting in embryonic lethality due to a defect in formation of yolk sac vasculature at E10.5 (Kaiser et al., 2011; Oberst et al., 2011; Varfolomeev et al., 1998; Zhang et al., 2011). As *CFLARs* Tg mice did survive at least until E16.5, the phenotype of *CFLARs* Tg mice is completely different from that of *Caspase 8*−/− or *Fadd*−/− mice. This might come from the timing of the expression of cFLIPs driven by the *CAG* promoter during development. In contrast, IEC-specific deletion of *Caspase 8* or *Fadd* (*Caspase* $8^{IEC\text{-}KO}$ or $Fadd^{IEC\text{-}KO}$) results in severe intestinal inflammation in mice after birth, suggesting that the phenotype of *CFLARs* Tg mice might be more severe than that of these murine models (Gunther et al., 2011; Welz et al., 2011). There are several differences among *CFLARs* Tg mice and these murine models. First, the development of ileitis in *CFLARs* Tg mice occurs earlier than other murine models, where the colitis usually starts after birth. Second, *CFLARs* Tg mice only developed ileitis, but *Caspase* $8^{IEC\text{-}KO}$ or $Fadd^{IEC\text{-}KO}$ mice develop both ileitis and colitis. Third, deletion of *Tnfsfr1a* did not rescue embryonic lethality of *CFLARs* Tg mice, whereas deletion of *Tnf* or *Tnfsfr1a* attenuates intestinal tissue injury in *Caspase* $8^{IEC\text{-}KO}$ or $Fadd^{IEC\text{-}KO}$ mice. Finally, large numbers of apoptotic cells were detected in the intestinal lumen, but very few apoptotic cells were detected in villi of *CFLARs* Tg mice. Although necroptosis was detected in various tissues, necroptotic cells per se were not sufficient to induce severe tissue damage in *CFLARs* Tg mice. Severe tissue damage of the SI of *CFLARs* Tg mice is tightly correlated with infiltration of ILC3s. Intriguingly, a recent study has reported that IL-22 enhances proliferation of IECs, but inhibits the expansion of intestinal stem cell (ISC)s, resulting in a decrease in organoid survival (Zwarycz et al., 2019). Thus it might be plausible that aberrantly produced IL-22 increases the turnover of IECs and suppresses the

expansion of ISCs, resulting in anoikis-dependent apoptosis of IECs in the SI of *CFLARs* Tg mice. Further study will be required to address this issue.

Approximately 10% population of extremely preterm infants spontaneously develops severe necrotizing enterocolitis (Lim et al., 2015; Tanner et al., 2015). The histology of necrotizing enterocolitis in human is characterized by the dilatation of the intestine, destruction of the villi structures, and intestinal bleeding. Intriguingly, these futures are reminiscent of the histological features of the SI of *CFLARs* Tg mice. Immaturity of host defense, type of infant feeding, ischemia, anatomical anomaly, and bacterial infection are considered to be responsible for the development of necrotizing enterocolitis. However, the detailed mechanisms remain unclear. As overexpression of cFLIPs induced ILC3s-dependent lethal ileitis, it would be interesting to test whether the expression of cFLIPs was increased in such patients. Given that IECs produce CCL20 in response to inflammatory cytokines such as TNF or IL-1β (Kwon et al., 2002), IECs might further recruit ILC3s, culminating in the development of lethal ileitis. Therefore it would be also intriguing to test whether ILC3s accumulate in the lesions of necrotizing enterocolitis in preterm infants.

Limitations of the Study

Our results demonstrate that blockade of necroptosis completely suppresses apoptosis of IECs, but only partially rescues embryonic lethality of *CFLARs* Tg mice. We do not currently know which pathway(s) other than necroptosis induces embryonic lethality of *CFLARs* Tg mice. Moreover, we cannot show genetic evidence that IL-22-dependent ROS production induces apoptosis of IECs of *CFLARs* Tg mice. Another limitation of our current study is the inability to answer whether the RORγt^{+} cells/IL-22 axis operates and contributes to the exacerbation of intestinal diseases in human patients. Further investigation will be required to address these issues.

METHODS

All methods can be found in the accompanying Transparent Methods supplemental file.

SUPPLEMENTAL INFORMATION

Supplemental Information can be found online at https://doi.org/10.1016/j.isci.2019.05.011.

ACKNOWLEDGMENTS

We thank M. Pasparakis for *Mlkl*−/− and *Ripk1*$^{DN/DN}$ mice, K. Honda for *Rorc-gfp/gfp* mice, V. Dixit and K. Newton for *Ripk3*−/− mice, Genentech, Inc. for *Il22*−/− mice, and T.W. Mak for *Tnfrsf1a*−/− mice. We thank H. Ohno and N. Sato for technical advice. R.S. was supported by a Research Fellowship from Japan Society for the Promotion of Science (JSPS), Japan. This work was supported in part by Grants-in-Aid from Scientific Research (B) 17H04069 (to H.N.) and Challenging Exploratory Research 17K19533 (to H.N.) from Japan Society for the Promotion of Science (JSPS) and Scientific Research on Innovative areas 26110003 (to H.N.), the Japan Agency for Medical Research and Development (AMED) through AMED-CREST with a grant number JP18gm1210002 (to H.N.), and Private University Research Branding project (to H.N.) from MEXT (Ministry of Education, Culture, Sports, Science and Technology), Japan.

AUTHOR CONTRIBUTIONS

Conceptualization, R.S., M.O., and H.N.; Investigation, R.S., S.K-S., S.M., Y.D., S.Y., T.N., S.K., and K.M.; Resources, M.O., T.Y., H. Konishi, H. Kiyama, T.M., and K.A.; Writing-Original Draft, R.S. and H.N.; Writing-Review & Editing, R.S., S.Y., K.M., and H.N.; Supervision, Y.U.

DECLARATION OF INTERESTS

The authors declare that they do not have competing financial interests. Data and Software Availability The accession number for the microarray data reported in this paper is NCBI GEO: GSE120982.

Received: January 28, 2019
Revised: April 12, 2019
Accepted: May 9, 2019
Published: May 31, 2019

REFERENCES

Bauche, D., Joyce-Shaikh, B., Jain, R., Grein, J., Ku, K.S., Blumenschein, W.M., Ganal-Vonarburg, S.C., Wilson, D.C., McClanahan, T.K., Malefyt, R.W., et al. (2018). LAG3(+) regulatory T cells restrain interleukin-23-producing CX3CR1(+) gut-resident macrophages during group 3 innate lymphoid cell-driven colitis. Immunity *49*, 342–352.e5.

Budd, R.C., Yeh, W.C., and Tschopp, J. (2006). cFLIP regulation of lymphocyte activation and development. Nat. Rev. Immunol. *6*, 196–204.

Buonocore, S., Ahern, P.P., Uhlig, H.H., Ivanov, I.I., Littman, D.R., Maloy, K.J., and Powrie, F. (2010). Innate lymphoid cells drive interleukin-23-dependent innate intestinal pathology. Nature *464*, 1371–1375.

Chan, F.K., Shisler, J., Bixby, J.G., Felices, M., Zheng, L., Appel, M., Orenstein, J., Moss, B., and Lenardo, M.J. (2003). A role for tumor necrosis factor receptor-2 and receptor-interacting protein in programmed necrosis and antiviral responses. J. Biol. Chem. *278*, 51613–51621.

Chen, L., He, Z., Slinger, E., Bongers, G., Lapenda, T.L., Pacer, M.E., Jiao, J., Beltrao, M.F., Soto, A.J., Harpaz, N., et al. (2015). IL-23 activates innate lymphoid cells to promote neonatal intestinal pathology. Mucosal Immunol. *8*, 390–402.

Christofferson, D.E., and Yuan, J. (2010). Necroptosis as an alternative form of programmed cell death. Curr. Opin. Cell Biol. *22*, 263–268.

Circu, M.L., and Aw, T.Y. (2010). Reactive oxygen species, cellular redox systems, and apoptosis. Free Radic. Biol. Med. *48*, 749–762.

Dannappel, M., Vlantis, K., Kumari, S., Polykratis, A., Kim, C., Wachsmuth, L., Eftychi, C., Lin, J., Corona, T., Hermance, N., et al. (2014). RIPK1 maintains epithelial homeostasis by inhibiting apoptosis and necroptosis. Nature *513*, 90–94.

Dillon, C.P., Oberst, A., Weinlich, R., Janke, L.J., Kang, T.B., Ben-Moshe, T., Mak, T.W., Wallach, D., and Green, D.R. (2012). Survival function of the FADD-CASPASE-8-cFLIP(L) complex. Cell Rep. *1*, 401–407.

Eberl, G., Marmon, S., Sunshine, M.J., Rennert, P.D., Choi, Y., and Littman, D.R. (2004). An essential function for the nuclear receptor RORgamma(t) in the generation of fetal lymphoid tissue inducer cells. Nat. Immunol. *5*, 64–73.

Eidenschenk, C., Rutz, S., Liesenfeld, O., and Ouyang, W. (2014). Role of IL-22 in microbial host defense. Curr. Top. Microbiol. Immunol. *380*, 213–236.

Eken, A., Singh, A.K., Treuting, P.M., and Oukka, M. (2014). IL-23R+ innate lymphoid cells induce colitis via interleukin-22-dependent mechanism. Mucosal Immunol. *7*, 143–154.

Esplugues, E., Huber, S., Gagliani, N., Hauser, A.E., Town, T., Wan, Y.Y., O'Connor, W., Jr., Rongvaux, A., Van Rooijen, N., Haberman, A.M., et al. (2011). Control of TH17 cells occurs in the small intestine. Nature *475*, 514–518.

Feoktistova, M., Geserick, P., Kellert, B., Dimitrova, D.P., Langlais, C., Hupe, M., Cain, K., MacFarlane, M., Hacker, G., and Leverkus, M. (2011). cIAPs block ripoptosome formation, a RIP1/caspase-8 containing intracellular cell death complex differentially regulated by cFLIP isoforms. Mol. Cell *43*, 449–463.

Grasberger, H., Gao, J., Nagao-Kitamoto, H., Kitamoto, S., Zhang, M., Kamada, N., Eaton, K.A., El-Zaatari, M., Shreiner, A.B., Merchant, J.L., et al. (2015). Increased expression of DUOX2 is an epithelial response to mucosal dysbiosis required for immune homeostasis in mouse intestine. Gastroenterology *149*, 1849–1859.

Gunther, C., Martini, E., Wittkopf, N., Amann, K., Weigmann, B., Neumann, H., Waldner, M.J., Hedrick, S.M., Tenzer, S., Neurath, M.F., et al. (2011). Caspase-8 regulates TNF-alpha-induced epithelial necroptosis and terminal ileitis. Nature *477*, 335–339.

Hao, Z., and Rajewsky, K. (2001). Homeostasis of peripheral B cells in the absence of B cell influx from the bone marrow. J. Exp. Med. *194*, 1151–1164.

Honda, K., and Littman, D.R. (2016). The microbiota in adaptive immune homeostasis and disease. Nature *535*, 75–84.

Kaiser, W.J., Upton, J.W., Long, A.B., Livingston-Rosanoff, D., Daley-Bauer, L.P., Hakem, R., Caspary, T., and Mocarski, E.S. (2011). RIP3 mediates the embryonic lethality of caspase-8-deficient mice. Nature *471*, 368–372.

Kobayashi, Y. (2008). The role of chemokines in neutrophil biology. Front. Biosci. *13*, 2400–2407.

Kwon, J.H., Keates, S., Bassani, L., Mayer, L.F., and Keates, A.C. (2002). Colonic epithelial cells are a major site of macrophage inflammatory protein 3alpha (MIP-3alpha) production in normal colon and inflammatory bowel disease. Gut *51*, 818–826.

Lim, J.C., Golden, J.M., and Ford, H.R. (2015). Pathogenesis of neonatal necrotizing enterocolitis. Pediatr. Surg. Int. *31*, 509–518.

Lyon, M.F. (1971). Possible mechanisms of X chromosome inactivation. Nature New Biol. *232*, 229–232.

Maloy, K.J., and Powrie, F. (2011). Intestinal homeostasis and its breakdown in inflammatory bowel disease. Nature *474*, 298–306.

Mandal, P., Berger, S.B., Pillay, S., Moriwaki, K., Huang, C., Guo, H., Lich, J.D., Finger, J., Kasparcova, V., Votta, B., et al. (2014). RIP3 induces apoptosis independent of pronecrotic kinase activity. Mol. Cell *56*, 481–495.

Manta, C., Heupel, E., Radulovic, K., Rossini, V., Garbi, N., Riedel, C.U., and Niess, J.H. (2013). CX(3)CR1(+) macrophages support IL-22 production by innate lymphoid cells during infection with Citrobacter rodentium. Mucosal Immunol. *6*, 177–188.

Mao, K., Baptista, A.P., Tamoutounour, S., Zhuang, L., Bouladoux, N., Martins, A.J., Huang, Y., Gerner, M.Y., Belkaid, Y., and Germain, R.N. (2018). Innate and adaptive lymphocytes sequentially shape the gut microbiota and lipid metabolism. Nature *554*, 255–259.

Matsumoto, S., Konishi, H., Maeda, R., Kiryu-Seo, S., and Kiyama, H. (2012). Expression analysis of the regenerating gene (Reg) family members Reg-IIIbeta and Reg-IIIgamma in the mouse during development. J. Comp. Neurol. *520*, 479–494.

Mortha, A., Chudnovskiy, A., Hashimoto, D., Bogunovic, M., Spencer, S.P., Belkaid, Y., and Merad, M. (2014). Microbiota-dependent crosstalk between macrophages and ILC3 promotes intestinal homeostasis. Science *343*, 1249288.

Murphy, J.M., Czabotar, P.E., Hildebrand, J.M., Lucet, I.S., Zhang, J.G., Alvarez-Diaz, S., Lewis, R., Lalaoui, N., Metcalf, D., Webb, A.I., et al. (2013). The pseudokinase MLKL mediates necroptosis via a molecular switch mechanism. Immunity *39*, 443–453.

Nakano, H., Piao, X., Shindo, R., and Komazawa-Sakon, S. (2017). Cellular FLICE-inhibitory protein regulates tissue homeostasis. Curr. Top. Microbiol. Immunol. *403*, 119–141.

Newton, K., Sun, X., and Dixit, V.M. (2004). Kinase RIP3 is dispensable for normal NF-kappa Bs, signaling by the B-cell and T-cell receptors, tumor necrosis factor receptor 1, and Toll-like receptors 2 and 4. Mol. Cell. Biol. *24*, 1464–1469.

Newton, K., Dugger, D.L., Wickliffe, K.E., Kapoor, N., de Almagro, M.C., Vucic, D., Komuves, L., Ferrando, R.E., French, D.M., Webster, J., et al. (2014). Activity of protein kinase RIPK3 determines whether cells die by necroptosis or apoptosis. Science *343*, 1357–1360.

O'Donnell, M.A., Perez-Jimenez, E., Oberst, A., Ng, A., Massoumi, R., Xavier, R., Green, D.R., and Ting, A.T. (2011). Caspase 8 inhibits programmed necrosis by processing CYLD. Nat. Cell Biol. *13*, 1437–1442.

Oberst, A., Dillon, C.P., Weinlich, R., McCormick, L.L., Fitzgerald, P., Pop, C., Hakem, R., Salvesen, G.S., and Green, D.R. (2011). Catalytic activity of the caspase-8-FLIP(L) complex inhibits RIPK3-dependent necrosis. Nature *471*, 363–367.

Ohnmacht, C. (2016). Tolerance to the intestinal microbiota mediated by ROR(gammat)(+) cells. Trends Immunol. *37*, 477–486.

Ouyang, W., and Valdez, P. (2008). IL-22 in mucosal immunity. Mucosal Immunol. *1*, 335–338.

Panayotova-Dimitrova, D., Feoktistova, M., Ploesser, M., Kellert, B., Hupe, M., Horn, S., Makarov, R., Jensen, F., Porubsky, S., Schmieder, A., et al. (2013). cFLIP regulates skin homeostasis and protects against TNF-induced keratinocyte apoptosis. Cell Rep. *5*, 397–408.

Parks, O.B., Pociask, D.A., Hodzic, Z., Kolls, J.K., and Good, M. (2015). Interleukin-22 signaling in the regulation of intestinal health and disease. Front. Cell Dev. Biol. *3*, 85.

Pasparakis, M., and Vandenabeele, P. (2015). Necroptosis and its role in inflammation. Nature *517*, 311–320.

Peltzer, N., Darding, M., Montinaro, A., Draber, P., Draberova, H., Kupka, S., Rieser, E., Fisher, A., Hutchinson, C., Taraborrelli, L., et al. (2018). LUBAC is essential for embryogenesis by preventing cell death and enabling haematopoiesis. Nature *557*, 112–117.

Pfeffer, K., Matsuyama, T., Kundig, T.M., Wakeham, A., Kishihara, K., Shahinian, A., Wiegmann, K., Ohashi, P.S., Kronke, M., and Mak, T.W. (1993). Mice deficient for the 55 kd tumor necrosis factor receptor are resistant to endotoxic shock, yet succumb to L. monocytogenes infection. Cell *73*, 45467.

Piao, X., Komazawa-Sakon, S., Nishina, T., Koike, M., Piao, J.H., Ehlken, H., Kurihara, H., Hara, M., Van Rooijen, N., Schutz, G., et al. (2012). c-FLIP maintains tissue homeostasis by preventing apoptosis and programmed necrosis. Sci. Signal. *5*, ra93.

Piao, X., Miura, R., Miyake, S., Komazawa-Sakon, S., Koike, M., Shindo, R., Takeda, J., Hasegawa, A., Abe, R., Nishiyama, C., et al. (2018). Blockade of TNF receptor superfamily 1 (TNFR1)-dependent and TNFR1-independent cell death is crucial for normal epidermal differentiation. J. Allergy Clin. Immunol. *143*, 213–228.e10.

Polykratis, A., Hermance, N., Zelic, M., Roderick, J., Kim, C., Van, T.M., Lee, T.H., Chan, F.K.M., Pasparakis, M., and Kelliher, M.A. (2014). Cutting edge: RIPK1 Kinase inactive mice are viable and protected from TNF-induced necroptosis in vivo. J. Immunol. *193*, 1539–1543.

Rickard, J.A., O'Donnell, J.A., Evans, J.M., Lalaoui, N., Poh, A.R., Rogers, T., Vince, J.E., Lawlor, K.E., Ninnis, R.L., Anderton, H., et al. (2014). RIPK1 regulates RIPK3-MLKL-driven systemic inflammation and emergency hematopoiesis. Cell *157*, 1175–1188.

Riedl, S.J., and Salvesen, G.S. (2007). The apoptosome: signalling platform of cell death. Nat. Rev. Mol. Cell Biol. *8*, 405–413.

Sakata, K., Araki, K., Nakano, H., Nishina, T., Komazawa-Sakon, S., Murai, S., Lee, G.E., Hashimoto, D., Suzuki, C., Uchiyama, Y., et al. (2016). Novel method to rescue a lethal phenotype through integration of target gene onto the X-chromosome. Sci. Rep. *6*, 37200.

Schattenberg, J.M., Zimmermann, T., Worns, M., Sprinzl, M.F., Kreft, A., Kohl, T., Nagel, M., Siebler, J., Bergkamen, H.S., He, Y.W., et al. (2011). Ablation of c-FLIP in hepatocytes enhances death-receptor mediated apoptosis and toxic liver injury in vivo. J. Hepatol. *55*, 1272–1280.

Shindo, R., Kakehashi, H., Okumura, K., Kumagai, Y., and Nakano, H. (2013). Critical contribution of oxidative stress to TNFalpha-induced necroptosis downstream of RIPK1 activation. Biochem. Biophys. Res. Commun. *436*, 212–216.

Taniwaki, T., Haruna, K., Nakamura, H., Sekimoto, T., Oike, Y., Imaizumi, T., Saito, F., Muta, M., Soejima, Y., Utoh, A., et al. (2005). Characterization of an exchangeable gene trap using pU-17 carrying a stop codon-beta geo cassette. Dev. Growth Differ. *47*, 163–172.

Tanner, S.M., Berryhill, T.F., Ellenburg, J.L., Jilling, T., Cleveland, D.S., Lorenz, R.G., and Martin, C.A. (2015). Pathogenesis of necrotizing enterocolitis: modeling the innate immune response. Am. J. Pathol. *185*, 4–16.

Tenev, T., Bianchi, K., Darding, M., Broemer, M., Langlais, C., Wallberg, F., Zachariou, A., Lopez, J., MacFarlane, M., Cain, K., et al. (2011). The Ripoptosome, a signaling platform that assembles in response to genotoxic stress and loss of IAPs. Mol. Cell *43*, 432–448.

Vaishnava, S., Yamamoto, M., Severson, K.M., Ruhn, K.A., Yu, X., Koren, O., Ley, R., Wakeland, E.K., and Hooper, L.V. (2011). The antibacterial lectin RegIIIgamma promotes the spatial segregation of microbiota and host in the intestine. Science *334*, 255–258.

Varfolomeev, E.E., Schuchmann, M., Luria, V., Chiannilkulchai, N., Beckmann, J.S., Mett, I.L., Rebrikov, D., Brodianski, V.M., Kemper, O.C., Kollet, O., et al. (1998). Targeted disruption of the mouse Caspase 8 gene ablates cell death induction by the TNF receptors, Fas/Apo1, and DR3 and is lethal prenatally. Immunity *9*, 267–276.

Vivier, E., Artis, D., Colonna, M., Diefenbach, A., Di Santo, J.P., Eberl, G., Koyasu, S., Locksley, R.M., McKenzie, A.N.J., Mebius, R.E., et al. (2018). Innate lymphoid cells: 10 years on. Cell *174*, 1054–1066.

Webster, J.D., Solon, M., Haller, S., and Newton, K. (2018). Detection of necroptosis by phospho-RIPK3 immunohistochemical labeling. Methods Mol. Biol. *1857*, 153–160.

Weinlich, R., Oberst, A., Beere, H.M., and Green, D.R. (2017). Necroptosis in development, inflammation and disease. Nat. Rev. Mol. Cell Biol. *18*, 127–136.

Welz, P.S., Wullaert, A., Vlantis, K., Kondylis, V., Fernandez-Majada, V., Ermolaeva, M., Kirsch, P., Sterner-Kock, A., van Loo, G., and Pasparakis, M. (2011). FADD prevents RIP3-mediated epithelial cell necrosis and chronic intestinal inflammation. Nature *477*, 330–334.

Wu, J., Huang, Z., Ren, J., Zhang, Z., He, P., Li, Y., Ma, J., Chen, W., Zhang, Y., Zhou, X., et al. (2013). Mlkl knockout mice demonstrate the indispensable role of Mlkl in necroptosis. Cell Res. *23*, 994–1006.

Yuan, J. (2006). Divergence from a dedicated cellular suicide mechanism: exploring the evolution of cell death. Mol. Cell *23*, 1–12.

Zhang, H., Zhou, X., McQuade, T., Li, J., Chan, F.K., and Zhang, J. (2011). Functional complementation between FADD and RIP1 in embryos and lymphocytes. Nature *471*, 373–376.

Zhang, N., and He, Y.W. (2005). An essential role for c-FLIP in the efficient development of mature T lymphocytes. J. Exp. Med. *202*, 395–404.

Zheng, Y., Valdez, P.A., Danilenko, D.M., Hu, Y., Sa, S.M., Gong, Q., Abbas, A.R., Modrusan, Z., Ghilardi, N., de Sauvage, F.J., et al. (2008). Interleukin-22 mediates early host defense against attaching and effacing bacterial pathogens. Nat. Med. *14*, 282–289.

Zwarycz, B., Gracz, A.D., Rivera, K.R., Williamson, I.A., Samsa, L.A., Starmer, J., Daniele, M.A., Salter-Cid, L., Zhao, Q., and Magness, S.T. (2019). IL22 inhibits epithelial stem cell expansion in an ileal organoid model. Cell. Mol. Gastroenterol. Hepatol. *7*, 1–17.

ISCI, Volume *15*

Supplemental Information

Necroptosis of Intestinal Epithelial Cells Induces Type 3 Innate Lymphoid Cell-Dependent Lethal Ileitis

Ryodai Shindo, Masaki Ohmuraya, Sachiko Komazawa-Sakon, Sanae Miyake, Yutaka Deguchi, Soh Yamazaki, Takashi Nishina, Takayuki Yoshimoto, Soichiro Kakuta, Masato Koike, Yasuo Uchiyama, Hiroyuki Konishi, Hiroshi Kiyama, Tetuo Mikami, Kenta Moriwaki, Kimi Araki, and Hiroyasu Nakano

ShindoFigS1

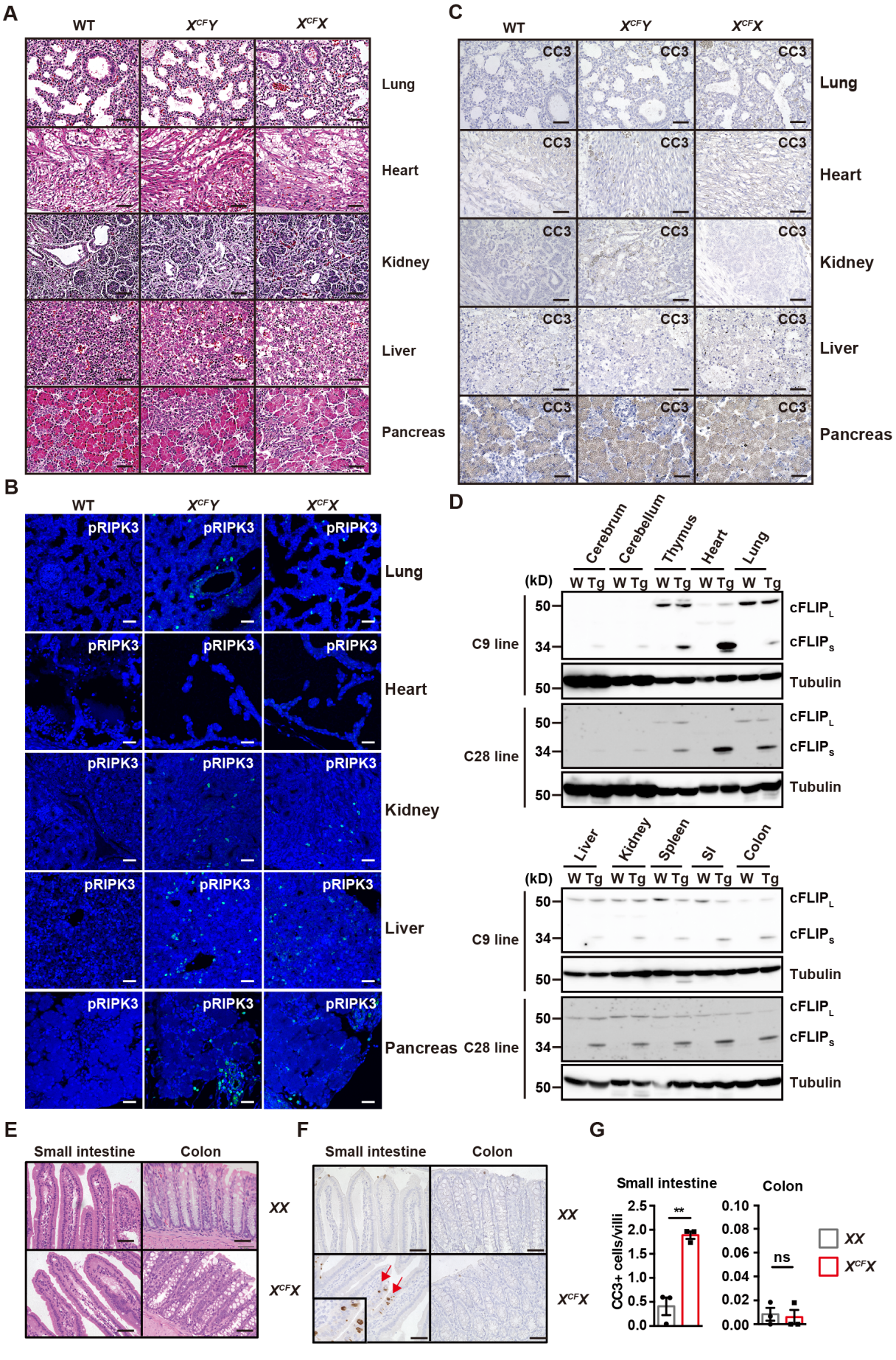

Figure S1. pRIPK3-, but not CC3-positive cells are detected in various tissues of *CFLARs* Tg mice, Related to Figure 1.

(A-C) Tissue sections from mice of the indicated genotypes at E18.5 were stained with H&E (A), anti-pRIPK3 (B), or anti-CC3 (C) antibodies (n=3 to 5 mice per each genotype). The tyramide signal amplification (TSA) method was used to enhance pRIPK3-positive signals. Scale bars, 50 μm.

(D) The expression of endogenous $cFLIP_L$ and exogenously introduced human cFLIPs in various tissues of 8-week-old $X^{CF}X$ mice. Extracts were prepared from various tissues and analyzed by immunoblotting with anti-cFLIP and anti-tubulin antibodies. C9 and C28 indicate two independently generated Tg lines. Results are representative of three independent experiments. W and Tg indicate WT and *CFLARs* Tg mice, respectively.

(E-G) Small numbers of IECs still undergo apoptosis in the SI of adult $X^{CF}X$ mice. Tissue sections of 6- to 8-week-old *XX* and $X^{CF}X$ mice were stained with H&E (E) or anti-CC3 antibody (F) (n= 3 to 5 mice per each genotype). The black box is an enlarged image of $CC3^+$ cells. $CC3^+$ cells are indicated by red arrows. Numbers of $CC3^+$ cells in the small intestine or colon were calculated in randomly selected fields (G). Results are expressed as numbers of $CC3^+$ cells per villi. Results are mean ± SEM (n=3 mice per each genotype). Statistical significance was determined by the two-tailed unpaired Student's *t* test. $^{**}P<0.01$; ns, not significant.

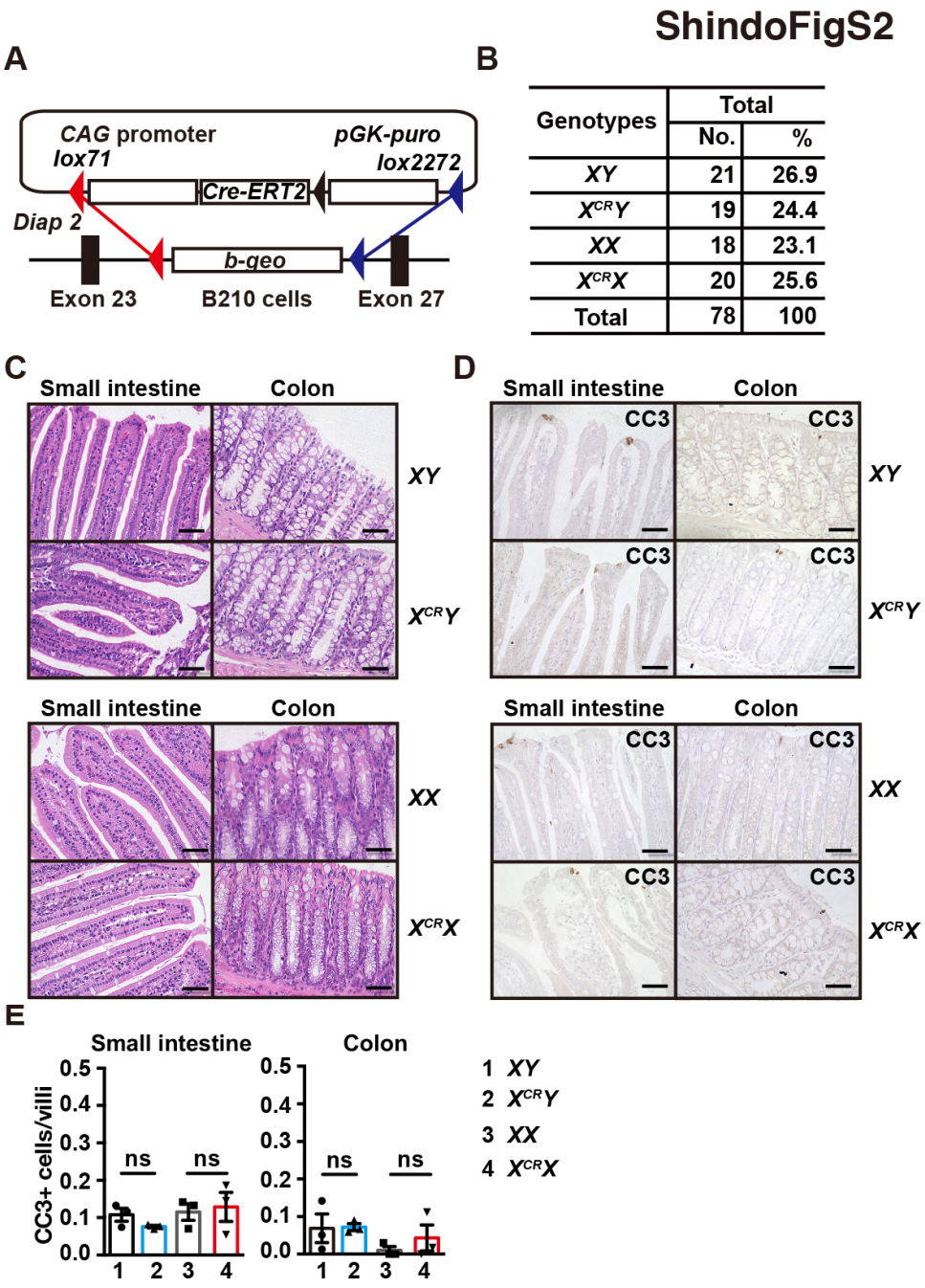

Figure S2. Inactivation of one allele of *Diap2* loci does not induce perinatal lethality, Related to Figure 1.

(A) Diagram of a vector for *Cre-ERT2* Tg mice.

(B) $X^{CR}Y$ mice are born at the expected Mendelian ratio and develop normally. The progeny of crossing male wild-type mice with $X^{CR}X$ mice. The genotypes of 2- to 4-week-old mice were determined by PCR.

(C-E) Small intestinal or colon sections of mice of the indicated genotypes at E18.5 were stained with H&E (C) (n=10 mice per each genotype) or anti-CC3 antibody (D) (n=3 to 4 mice per each genotype). Scale bars, 100 μm. Numbers of $CC3^+$ cells were counted and are expressed as in Figure S1G (E). Results are mean ± SEM (n=3 mice per group). Statistical significance was determined by the two-tailed unpaired Student's *t* test. ns, not significant.

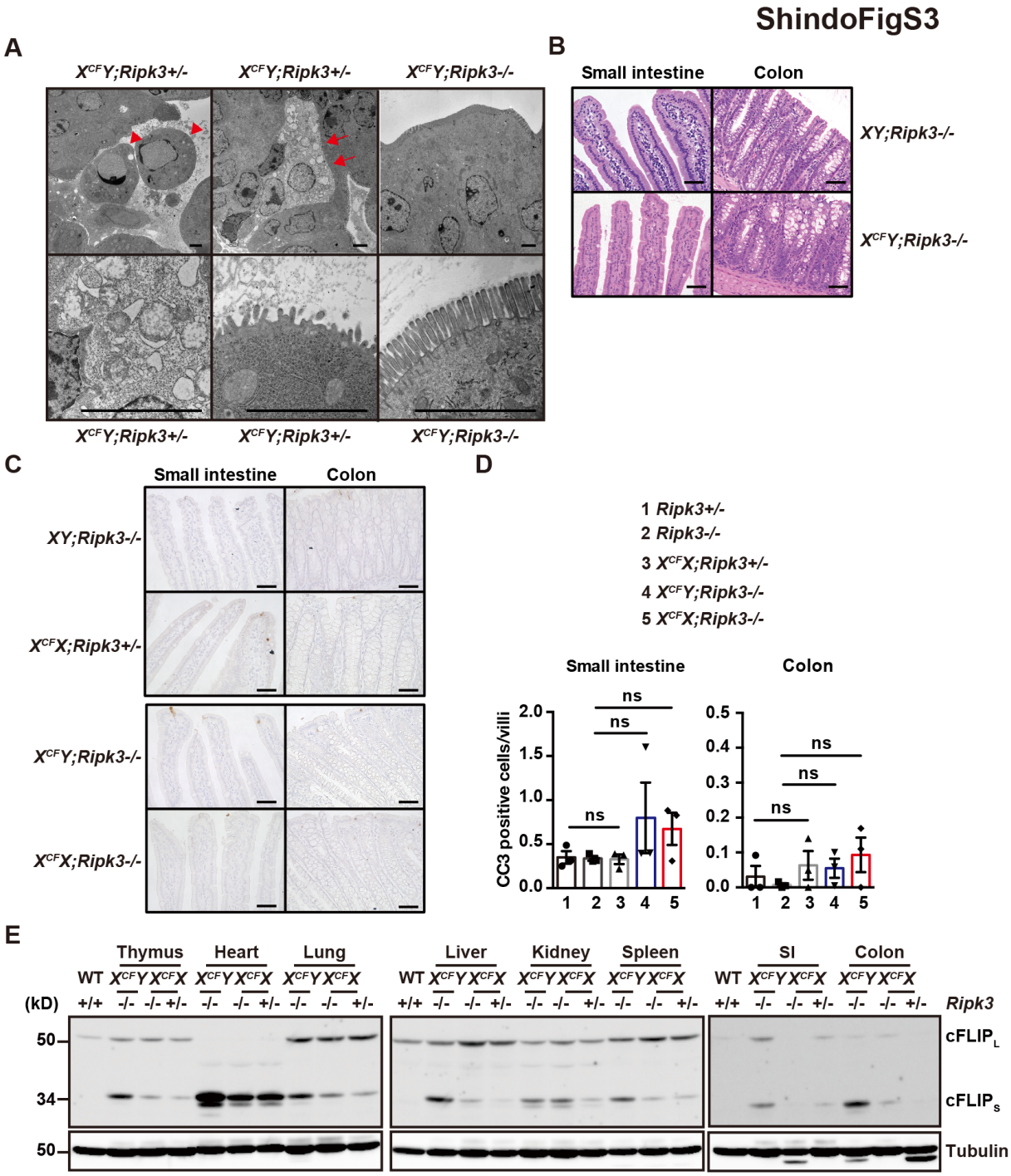

Figure S3. Male *CFLARs* Tg;*Ripk3*-/- mice grow without apparent abnormality, Related to Figure 3.

(A) Transmission electron microscopic analysis of the SI of mice of the indicated genotypes at E18.5. Results are representative of two independent experiments. Scale bars, 5 μm. Red arrowheads and arrows indicate apoptotic and necroptotic cells, respectively.

(B-D) Small intestinal sections from 6- to 8-week-old mice of the indicated genotypes were stained with H&E (B) or anti-CC3 antibody (C) (n= 3 mice per each genotype). Scale bars, 100 μm. Numbers of $CC3^{+}$ cells were counted and are expressed as in Figure S1G (D). Results are mean ± SEM (n=3 mice

per each genotype). Statistical analysis was determined by the one-way ANOVA test. ns, not significant.

(E) Expression of cFLIPs in various tissues. Tissue extracts from mice of the indicated genotype were analyzed by immunoblotting with anti-cFLIP and anti-tubulin antibodies. Results are representative of two independent experiments.

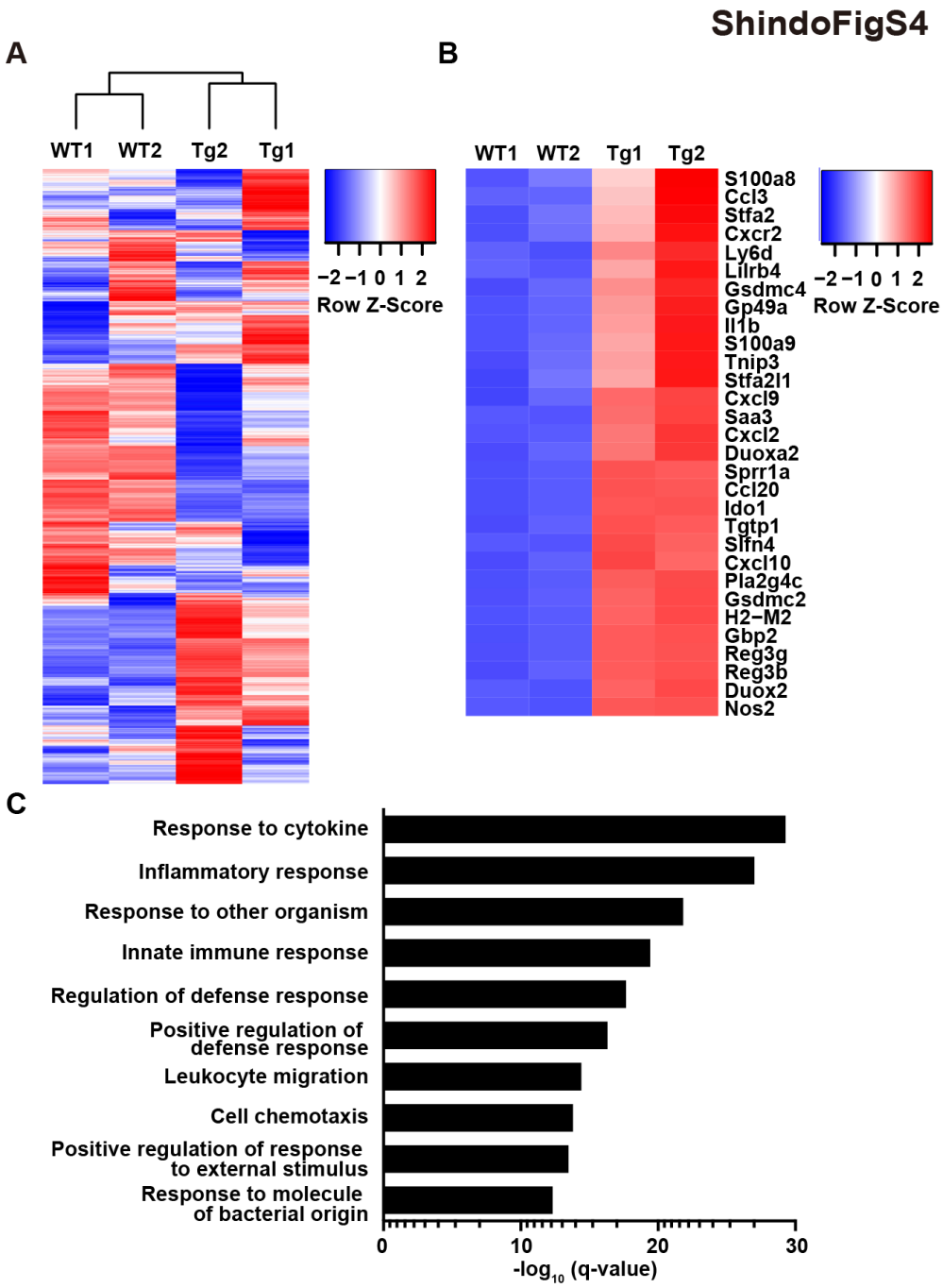

Figure S4. Transcriptome analysis of the SI of *CFLARs* Tg mice, Related to Figure 5.

(A) RNAs were prepared from the SI of mice of the indicated genotype at E18.5, and the expression of genes was determined by microarray analysis. Heat map of microarray gene expression of the SI of the indicated mice and their clustering are shown. Gene-expression color normalized by Z score transformation is shown at the right.

(B) Heat map of 30 genes upregulated more than two-fold in *CFLARs* Tg mice compared to WT mice. Red and blue indicate higher and lower relative expression, respectively.

(C) Signaling pathways significantly enriched in the SI of *CFLARs* Tg mice compared to wild-type mice.

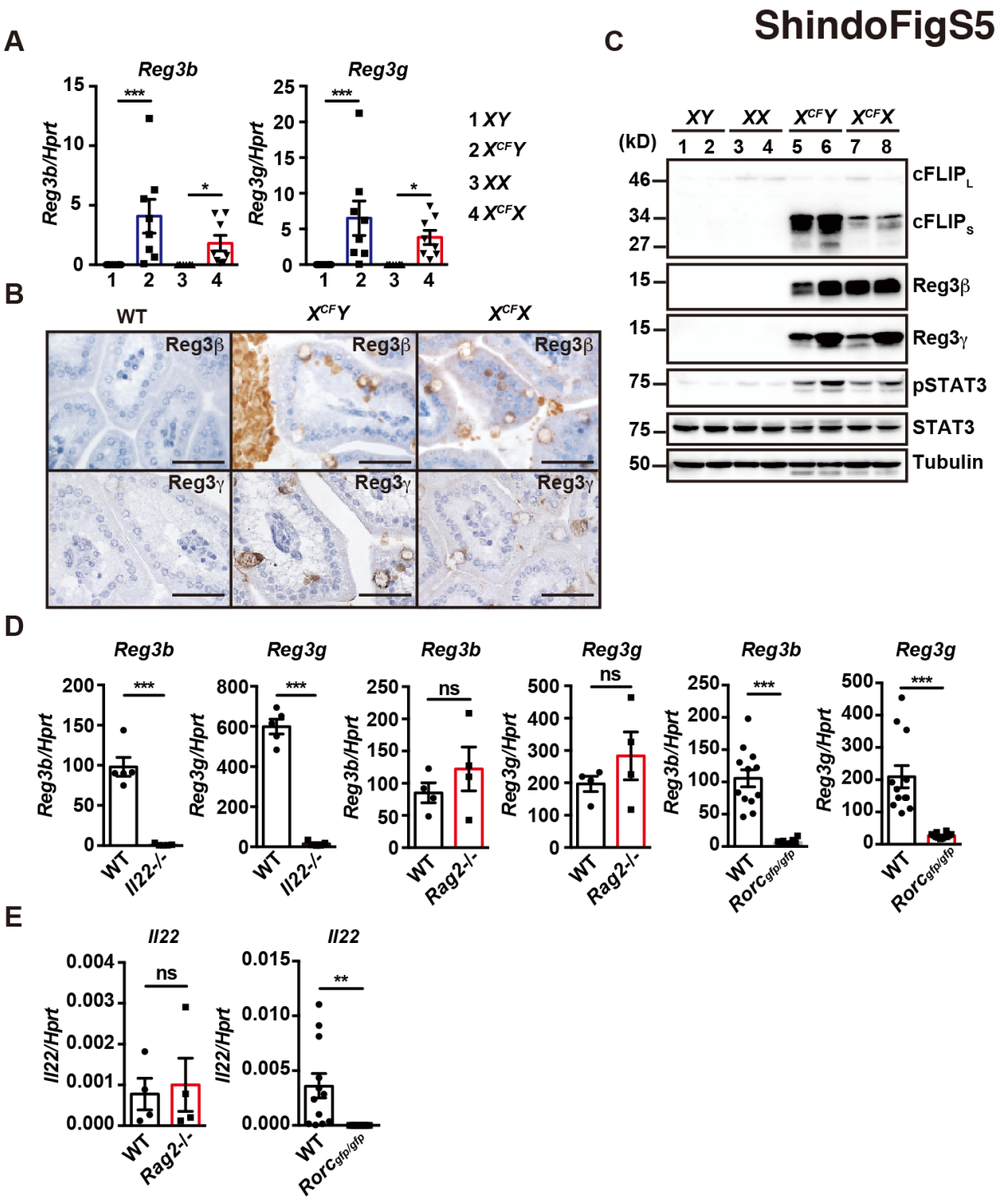

Figure S5. Expression of *Reg3b* and *Reg3g* is elevated in the SI of *CFLARs* Tg mice, Related to Figure 5.

(A) mRNAs were extracted from the SI of mice of the indicated genotypes at E18.5, and the expression of *Reg3b* and *Reg3g* were determined by qPCR. Results are mean ± SEM (n=8 mice per each genotype). Statistical significance was determined by the two-tailed unpaired Student's *t* test. **P*<0.05; ****P*<0.001.

(B) Small intestinal sections of mice of the indicated genotypes at E18.5 were stained with anti-Reg3β or anti-Reg3γ antibodies (n=3 mice per each genotype). Scale bars, 100 μm. Results are representative of three independent experiments.

(C) Tissue extracts of the SI of mice of the indicated genotypes at E18.5 were analyzed by immunoblotting with the indicated antibodies (n=2 mice per each genotype). Each number indicates an individual mouse. Results are representative of two independent experiments.

(D) The expression of *Reg3b* and *Reg3g* mRNAs is abolished in the SI of mice on an *Il22*-/-, or *Rorc-gfp/gfp*, but not *Rag2*-/- background. mRNAs were prepared from the SI of 8- to 12-week-old mice of the indicated genotypes, and the expressions of *Reg3b* and *Reg3g* was determined by qPCR. Results are mean ± SEM (n= 4 to 12 per group). Statistical significance was determined by the two-tailed unpaired Student's t test. ***$P<0.001$; ns, not significant. (E) The expression of *Il22* mRNAs is abolished in the SI of *Rorc-gfp/gfp*, but not *Rag2*-/- mice. mRNAs were prepared as in (D), the expressions of *Il22* was determined by qPCR. Results are mean ± SEM (n= 4 to 12 per group). Statistical significance was determined by the two-tailed unpaired Student's t test. **$P<0.01$; ns, not significant.

ShindoFigS6

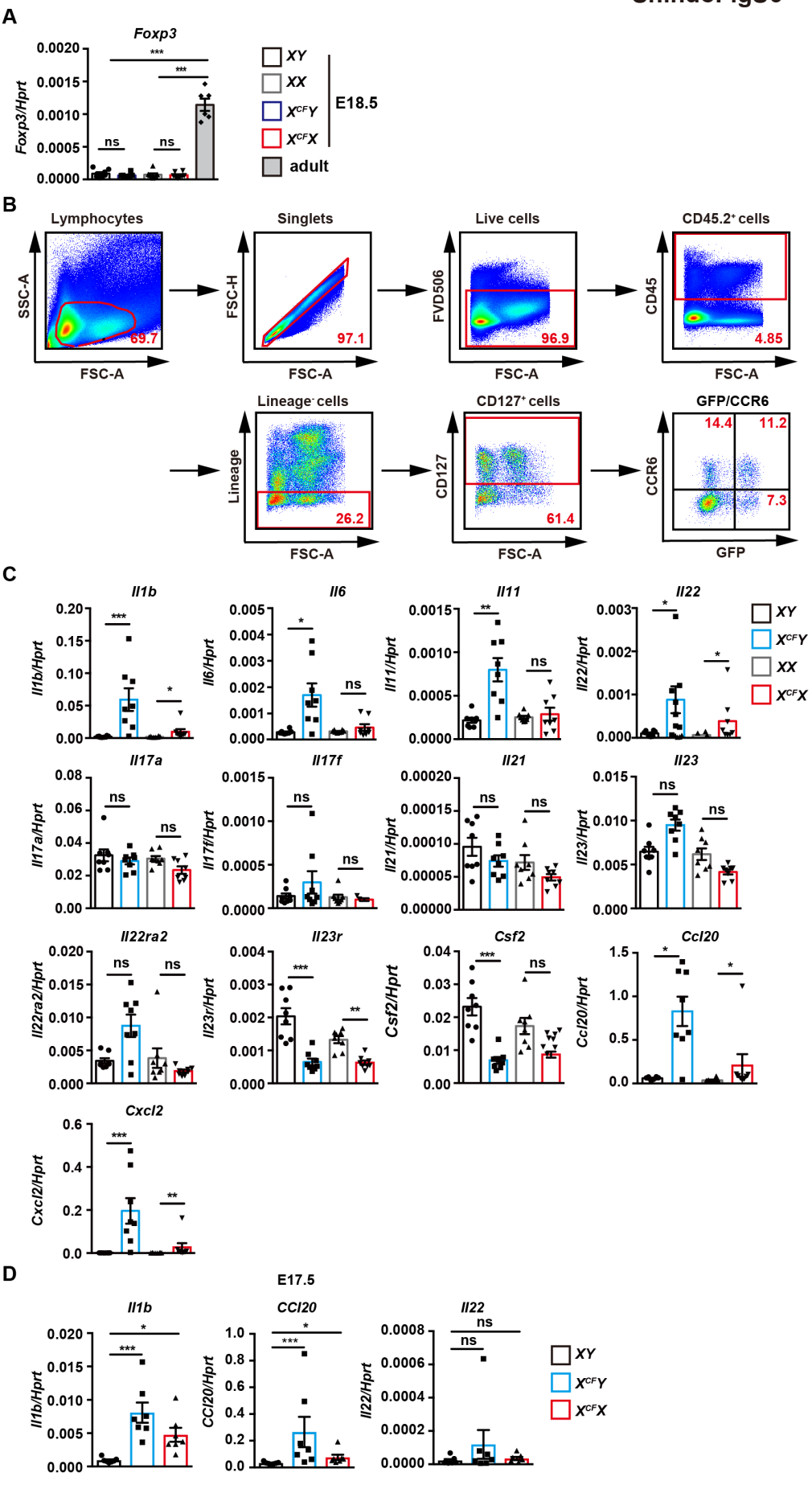

Figure S6. Gating strategy to analyze RORγt$^+$ ILCs and expression of ILC3 signature genes in the SI of *CFLARs* Tg mice, Related to Figure 5.

(A, C, D) RNAs were prepared from the SI of mice of the indicated genotypes at E18.5 (A, C) or E17.5 (D) or 8- to 12-week-old wild-type adult mice (A), and the expression of the indicated genes was determined by qPCR. Results are mean ± SEM (n=6 to 8 mice per each genotype). Statistical significance was determined by the two-tailed unpaired Student's *t* test. **P*<0.05; ***P*<0.01; ****P*<0.001; ns, not significant.

(B) Gating strategy of analysis of RORγt$^+$ ILC3s. Intestinal lamina propria cells were isolated as described in Transparent Methods. Live and CD45.2$^+$ cells were gated, and then lineage-negative cells were gated. CD127$^+$ cells were analyzed by the expression of GFP and CCR6. Representative results of three independent pooled experiments.

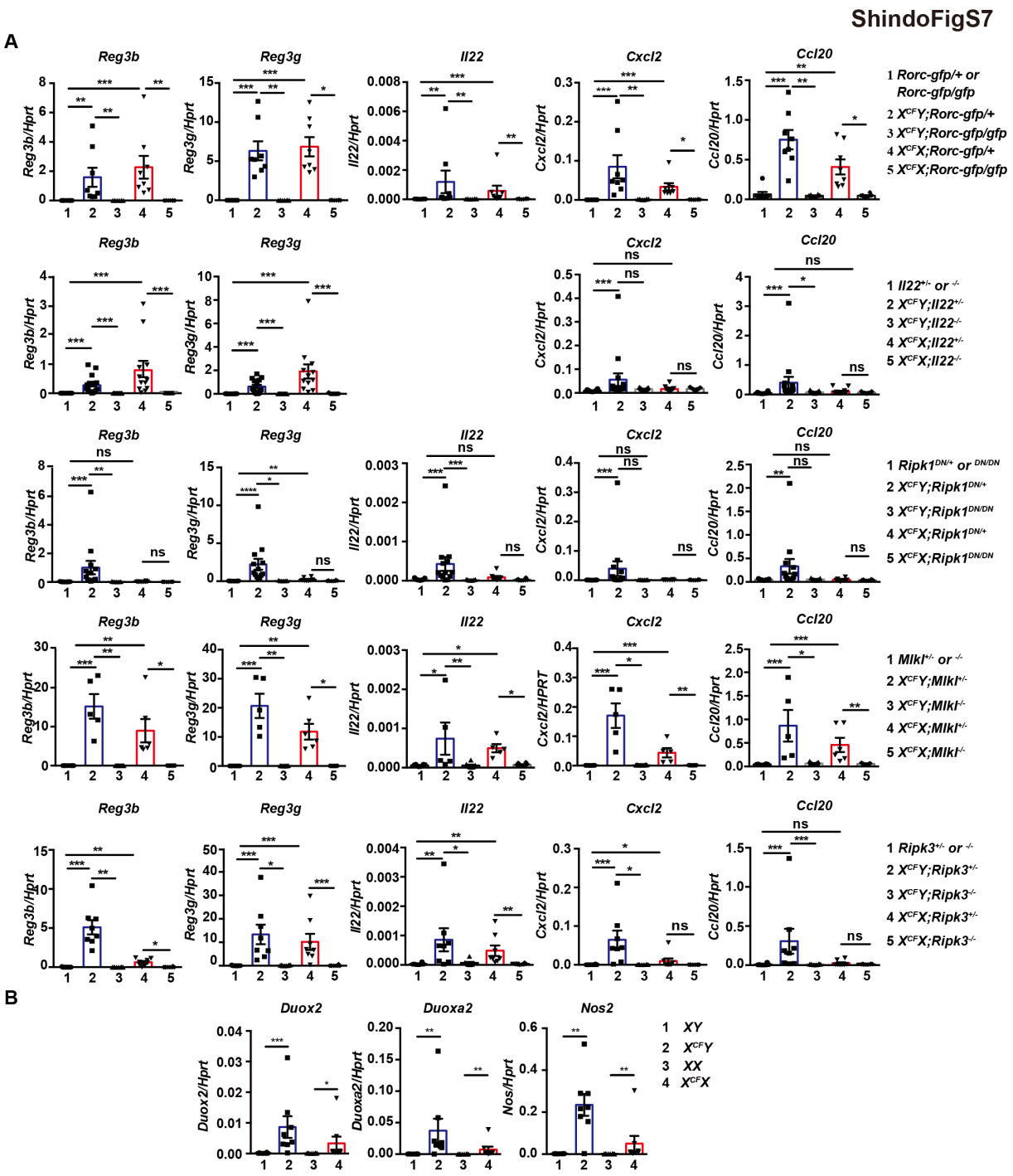

Figure S7. Deletion of genes associated with necroptosis, *Il22,* or *Rorc* downregulates the expression of various genes in the SI of *CFLARs* Tg mice, Related to Figure 6.

(A, B) mRNAs were prepared from the SI of mice of the indicated genotypes at E18.5, and the expression of the indicated genes was determined by qPCR. Results are mean ± SEM (n=5 to 15 mice per group). Statistical analysis was determined by the one-way ANOVA test (A) or the two-tailed unpaired Student's *t* test (B). **P*<0.05; ***P*<0.001; ****P*<0.001; ns, not significant.

Table S1. Upregulated genes in the SI of *CFLARs* Tg mice compared to wild-type mice, Related to Figure 5.

Accession No.	Symbol	Gene	Fold change
NM_011260	*Reg3g*	regenerating islet-derived 3 gamma	48.5
NM_011036	*Reg3b*	regenerating islet-derived 3 beta	35.1
NM_008204	*H2-M2*	histocompatibility 2, M region locus 2	21.4
NM_009140	*Cxcl2*	chemokine (C-X-C motif) ligand 2	21.1
NM_011315	*Saa3*	serum amyloid A 3	19.6
NM_0011685	*Pla2g4c*	phospholipase A2, group IVC (cytosolic, calcium-independent)	18.7
NM_008599	*Cxcl9*	chemokine (C-X-C motif) ligand 9	12.8
NM_010927	*Nos2*	nitric oxide synthase 2, inducible	11.6
NM_0011682	*Gsdmc2*	gasdermin C2	11.3
NM_177610	*Duox2*	dual oxidase 2	11.0
NM_028992	*Gsdmc4*	gasdermin C4	10.4
NM_173869|	*Stfa2l1*	stefin A2 like 1	10.3
NM_0011682	*Gsdmc2*	gasdermin C2	9.3
NM_016960|	*Ccl20*	chemokine (C-C motif) ligand 20	8.5
NM_008324	*Ido1*	indoleamine 2,3-dioxygenase 1	8.4
NM_0010825	*Stfa2*	stefin A2	8.3
NM_025777	*Duoxa2*	dual oxidase maturation factor 2	7.8
NM_010260	*Gbp2*	guanylate binding protein 2	7.6
NM_021274	*Cxcl10*	chemokine (C-X-C motif) ligand 10	7.3
NM_008147	*Gp49a*	glycoprotein 49 A	7.1
NM_011410	*Slfn4*	schlafen 4	6.9
NM_011337	*Ccl3*	chemokine (C-C motif) ligand 3	6.9
NM_011579|	*Tgtp1*	T-cell specific GTPase 1	6.7
NM_009114	*S100a9*	S100 calcium binding protein A9 (calgranulin B)	6.6
NM_0010825	*BC100530*	cDNA sequence BC100530	6.5
NM_009264	*Sprr1a*	small proline-rich protein 1A	6.5
NM_011579	*Tgtp1*	T-cell specific GTPase 1	6.4

NM_013650	*S100a8*	S100 calcium binding protein A8 (calgranulin A)	6.4
NM_144544	*2210407C*	RIKEN cDNA 2210407C18 gene	6.3
NM_0010014	*Tnip3*	TNFAIP3 interacting protein 3	5.8
NM_008361	*Il1b*	interleukin 1 beta	5.7
NM_013532	*Lilrb4*	leukocyte immunoglobulin-like receptor, subfamily B, member 4	5.6
NM_008392	*Irg1*	immunoresponsive gene 1	5.4
NM_009909	*Cxcr2*	chemokine (C-X-C motif) receptor 2	5.4
NM_010742	*Ly6d*	lymphocyte antigen 6 complex, locus D	5.3
NM_008530	*Ly6f*	lymphocyte antigen 6 complex, locus F	5.1
NM_011113	*Plaur*	plasminogen activator, urokinase receptor	5.0
NM_153564	*Gbp5*	guanylate binding protein 5	4.9
NM_0011462	*Iigp1*	interferon inducible GTPase 1	4.9
NM_010416	*Hemt1*	hematopoietic cell transcript 1	4.8
NM_0011360	*Anxa10*	annexin A10	4.7
NM_0011682	*Serpina3f*	serine (or cysteine) peptidase inhibitor, clade A, member 3F	4.7
NM_0010819	*Gm11428*	predicted gene 11428	4.7
NM_009903	*Cldn4*	claudin 4	4.7
NM_0010256	*Il1rl1*	interleukin 1 receptor-like 1	4.6
NM_009704	*Areg*	amphiregulin	4.6
NM_007607	*Car4*	carbonic anhydrase 4	4.6
NM_008620	*Gbp4*	guanylate binding protein 4	4.5
NM_010555	*Il1r2*	interleukin 1 receptor, type II	4.4
NM_008611	*Mmp8*	matrix metallopeptidase 8	4.4
NM_008491	*Lcn2*	lipocalin 2	4.3
NM_009252	*Serpina3n*	serine (or cysteine) peptidase inhibitor, clade A, member 3N	4.3
NM_0010332	*Nlrc5*	NLR family, CARD domain containing 5	4.1
NM_011452	*Serpinb9b*	serine (or cysteine) peptidase inhibitor, clade B, member 9b	4.1
NM_181596	*Retnlg*	resistin like gamma	4.1

RNAs were extracted from the SI of the indicated mice at E18.5 and analyzed using oligonucleotide arrays. Fold changed were calculated using the expression levels of each gene in the SI of *CFLARs* Tg mice compared to those of wild-type mice and top 55 genes are shown. Experiments were performed using two mice per each genotype and the average values of fold change are shown.

Table S2. **Primers used for qPCR in the study, Related to Figure 5.**

Ccl20:	5'- GCCTCTCGTACATACAGACGC-3'
	5'- CCAGTTCTGCTTTGGATCAGC-3'
Csf2:	5'- CTTTGAATGCAAAAAACCAGTCC-3'
	5'- TCCTGGCTCATTACGCAGGC-3'
Cxcl2:	5'- CCAACCACCAGGCTACAGG-3'
	5'- GCGTCACACTCAAGCTCTG-3'
Duox2:	5'- ACGCAGCTCTGTGTCAAAGGT-3'
	5'- TGATGAACGAGACTCGACAGC-3'
Duoxa2:	5'-GACGGGGTGCTACCCTTTTAC-3'
	5'-GCTAAGAAGGACTCTCACCAAC-3'
Foxp3:	5'-GGCGAAAGTGGCAGAGAGG-3'
	5'-AAGGCAGAG TCAGGAGAAGTTG-3'
Hprt:	5'- AACAAAGTCTGGCCTGTATCCAA -3'
	5'- GCAGTACAGCCCCAAAATGG-3'
Il1b:	5'- GCAACTGTTCCTGAACTCAACT-3'
	5'- ATCTTTTGGGGTCCGTCAACT-3'
Il6:	5'- GTATGAACAACGATGATGCACTTG-3'
	5'- ATGGTACTCCAGAAGACCAGAGGA-3'
Il11:	5'- CTGCACAGATGAGAGACAAATTCC-3'
	5'- GAAGCTGCAAAGATCCCAATG-3'
Il17a:	5'- CTGGAGGATAACACTGTGAGAGT-3'
	5'- TGCTGAATGGCGACGGAGTTC-3'
Il17f:	5'- CAAAACCAGGGCATTTCTGT-3'
	5'- ATGGTGCTGTCTTCCTGACC-3'
Il21:	5'- AGCCCCCAAGGGCCAGATCGC-3'
	5'- AGCTGCATGCTCACAGTGCCCCTTT-3'
Il22:	5'- TCCGAGGAGTCAGTGCTAAA-3'
	5'- AGAACGTCTTCCAGGGTGAA-3'
Il22ra2:	5'-TCAGCAGCAAAGACAGAAGAAAC-3'
	5'-GTGTCTCCAGCCCAACTCTCA-3'

Il23:	5’-GGGGAACATTATACTTTCCTGG-3’
	5’-CTAGATTCT GTTAGAACTGAGG-3’
Il23r:	5’-CCCAG ACAGTTTCCCAGGTTACAGC-3’
	5’-TGGCCAAGAAGACCATTCCCGACA-3’
Nos2:	5’-GTTCTCAGCCCAACAATACAAGA-3’
	5’-GTGGACGGGTCGATGTCAC-3’
Reg3b:	5’- CTCCTGCCTGATGCTCTTAT-3’
	5’- TTGTTACTC-CATTCCCATCC-3’
Reg3g:	5’- ACGAATCCTTCCTCTTCCTCAG-3’
	5’- GTCTTCACATTTGGGATCTTG-C-3’

Transparent Methods

Reagents

Murine TNF (34-8321, eBioscience), zVAD-fmk (3188-v, Peptide Institute), and Hoechst 33258 (Molecular Probes) were purchased from the indicated sources. The following antibodies were used in this study and were obtained from the indicated sources: anti-Reg3β (AF5110, R&D Systems, 1: 3000 for WB, 1: 200 for IHC), anti-cFLIP (Dave-2, Adipogen, 1: 500 for WB, 1: 200 for IF), anti-caspase-3 (9662, Cell Signaling, 1: 1000), anti-cleaved caspase-3 (9661, Cell Signaling, 1: 1000 for WB, 1: 200 for IHC or IF), anti-caspase-8 (1G12, Alexis, 1: 1000), anti-CCL20 (MAB7601, R&D SYSTEMS, 1: 200), anti-F4/80 (BM8, Caltag, 1: 100), anti-RIPK3 (IMG-5523-2, IMGENEX, 1: 3000), anti-phospho-RIPK3 (57220, Cell Signaling, 1: 1000 for WB, 1: 200 for IF), anti-tubulin (T5168, Sigma-Aldrich, 1: 40000), anti-STAT3 (sc-482, Santa-Cruz, 1: 1000), anti-phospho-STAT3 (9131, Cell Signaling, 1: 1000), anti-CD3 (Ab5690, Abcam, 1: 200) were purchased from the indicated sources. Anti-CD3 (145-2C11, 1: 200), anti-CD4 (RM4-5, 1: 200), anti-CD8 (53-6.7, 1: 200), anti-CD11b (M1/70, 1: 200), anti-CD11c (N418, 1: 200), anti-CD19 (1D3, 1: 200), anti-B220 (RA3-6B2, 1: 200), anti-Gr-1 (RB6-8C5, 1: 200), anti-Ly-6G (1A8, 1: 200), anti-CD45.2 (104, 1: 100), anti-TER-119 (TER-119, 1: 200), anti-CD127 (A7R34, 1: 200) antibodies were purchased from TONBO Biosciences. Anti-CCR6 antibody (140706, 1: 200) and Fixable Viability Dye eFluor 506 (65-0816-14) were purchased from BD and eBioscience. Anti-Reg3β (1: 1000) and anti-Reg3γ (1: 1000) antibodies were described previously (Matsumoto et al., 2012). HRP-conjugated donkey anti-rabbit IgG (NA934, 1:5000), HRP-conjugated sheep anti-mouse IgG (NA931, 1: 5000), HRP-conjugated goat anti-rat IgG (NA935, 1: 5000) antibodies were purchased from GE Healthcare Life Science. Alexa Fluor 594–conjugated donkey anti-rabbit IgG (A21207, 1: 500) and Alexa Fluor 488-conjugated donkey anti-goat IgG (A11055, 1: 500) antibodies were from Invitrogen. Biotin-conjugated goat anti-rabbit IgG (E0432, Dako, 1: 200), Biotin-conjugated rabbit anti-rat IgG (BA-4001, VECTOR, 1: 200) and biotin-conjugated rabbit anti-sheep IgG (BA-6000, VECTOR, 1: 200) antibodies, and HRP-conjugated streptavidin (P0397, Dako, 1: 300) were purchased from the indicated sources.

Cells

Primary MEFs were prepared from mice of the indicated genotypes at E14.5 after coitus using a standard method. MEFs below ten passages were used as primary MEFs for experiments. MEFs were maintained with DMEM containing 10% fetal calf serum.

Cell viability assay

MEFs were plated onto 96-well plates and cultured for 12 hours in DMEM containing 10% FCS. Then, cells were stimulated with the indicated concentrations of TNF in the absence or presence of zVAD-fmk

(20 μM) for 7 hours. Cell viability was determined by WST-1 (water soluble 2-(4-iodophenyl)-3-(4-nitrophenyl)-5-(2,4-disulfophenyl)[2H] tetrazolium monosodium salt-1) assay using a Cell Counting kit (343-07623, Dojindo).

Mice

Ripk3-/- (Newton et al., 2004) (provided by V. Dixit), *Mlkl*-/- (Dannappel et al., 2014) and *Ripk1*$^{DN/DN}$ (Polykratis et al., 2014) (provided by M. Pasparakis), *Il22*-/- (Zheng et al., 2008) (provided by Genentech, Inc.), and *Tnfrsf1a*-/- (Pfeffer et al., 1993) (provided by T.W. Mak) mice were described previously. *Rorc-gfp/gfp* mice (Eberl et al., 2004) were provided by K. Honda under the third party transfer agreement of the Jackson Lab. *Rag2*-/- mice (Hao and Rajewsky, 2001) were purchased from the Jackson Lab. C57/BL6 mice were purchased from Sankyo Lab. All experiments were performed according to the guidelines approved by the Institutional Animal experiments Committee of Kumamoto University, Juntendo University Graduate School of Medicine, Toho University School of Medicine, and Tokyo Medical University.

Generation of *CFLARs* Tg mice at the *Diap2* locus on the X-chromosome

We previously generated one ES cell line designated B210, in which a promoter trap vector was integrated into the *Diaphanous homolog 2 (Diap2)* gene on the X-chromosome (Taniwaki et al., 2005). We transfected a replacement vector for *CFLARs* where the expression of *CFLARs* was under the control of the *cytomegalovirus early enhancer/chicken b-actin (CAG)* promoter and flanked by two mutant *lox* sites into B210 cells (Figure 1A). The replacement vector was electroporated into B210 cells along with an expression vector for *Cre recombinase* to induce recombination between two mutant *lox* sites. Characterization of B210 ES cells harboring a gene trap vector at the *Diap2* locus on the X-chromosome will be published elsewhere. Selection was maintained for 5 days, and then colonies were picked into 48-well plates and expanded for freezing. The puromycin-resistant colonies were analyzed by Southern blotting and PCR to select ES cell lines showing successful integration of p*CAGGS-CFLARs*-pA. Positive clones were aggregated with ICR morula according to the protocol previously described. Germline transmission was obtained in three mouse lines, and two different lines were backcrossed onto C57BL/6N at least 5 generations. *CFLARs* Tg mouse lines, designated as C9 and C28, were used in this study.

Cre-ERT2 Tg mice were generated by an essentially similar to the protocol of generation of *CFLARs* Tg mice as described above. Detailed information of a vector of p*CAGGS-Cre-ERT2*-pA and characterization of *Cre-ERT2* Tg mice will be published elsewhere.

Western blotting

Murine tissues were homogenized with a Polytron (KINEMATICA) or cells were lysed in RIPA buffer [50 mM Tris-HCl (pH 8.0), 150 mM NaCl, 1% Nonidet P-40, 0.5% deoxycholate, 0.1% SDS, 25 mM β-glycerophosphate, 1 mM sodium orthovanadate, 1 mM sodium fluoride, 1 mM phenylmethylsulfonyl fluoride (PMSF), 1 μg/ml aprotinin, and 1 μg/ml leupeptin]. After centrifugation, tissue extracts or cell lysates were subjected to SDS polyacrylamide gel electrophoresis (SDS-PAGE) and transferred onto polyvinylidene difluoride (PVDF) membranes (Millipore). The membranes were analyzed with the indicated antibodies. The membranes were developed with Super Signal West Dura Extended Duration Substrate (Thermo Scientific) and analyzed with a LAS4000 or Amersham Imager 600 (GE Healthcare Life Sciences).

Histological, immunohistochemical, and immunofluorescence analyses

Murine tissues were fixed in 10% formalin and embedded in paraffin blocks. Paraffin-embedded tissue sections were used for hematoxylin and eosin (H&E) staining. TUNEL staining was performed with ApopTag Fluorescein *In Situ* Apoptosis Detection kit (S7110, Millipore) (for Figure 1G) or the *In Situ* Detection kit (Roche Diagnostics) (for Figure 2E). Briefly, paraffin-embedded sections were incubated with a TdT reaction mixture containing digoxigenin nucleotide and biotin-16-dUTP followed by incubation with fluorescein-conjugated anti-digoxigenin antibody and HRP–conjugated streptavidin, respectively. For immunostaining, paraffin-embedded sections were incubated with the indicated primary antibodies and then visualized with respective secondary antibodies. To detect cFLIPs, pRIPK3, Gr-1, and CCL20, the tyramide signal amplification (TSA) method was applied according to the manufacturer's instructions (NEL741001KT, PerkinElmer). Images were obtained by All In One analyzer (KEYENCE) or confocal microscopy (Nikon). Images were analyzed with KEYENCE software (KEYENCE) or NIS-Elements AR Analysis software (Nikon).

TEM analysis

Small intestines from mice of the indicated genotype at E17.5 or E18.5 were removed and fixed with 2% glutaraldehyde and 2% paraformaldehyde in 0.1 M phosphate buffer, pH 7.4. Slices of these fixed tissues were postfixed with 2% OsO_4, dehydrated in ethanol, and embedded in Epok 812 (Okenshoji Co.). Ultrathin sections were cut with an ultramicrotome (ultracut N or UC6: Leica), stained with uranyl acetate and lead citrate, and examined with a Hitachi HT7700 or JEOL JEM-1400 electron microscope.

Microarray analysis

We compared gene expression profiles of RNAs from the intestines of wild-type and *CFLARs* Tg mice at E18.5. Total RNAs were extracted from the small intestines of mice of the indicated genotype at E18.5 (n=2 mice per each genotype) using Sepasol-RNA I Super G according to the manufacturer's

instructions (09379-55, Nacalai Tesque), then labeled with Cy3. Samples were hybridized to a Mouse Oligonucleotide Microarray (G4121B, Agilent) according to the manufacturer's protocol. Arrays were scanned with a G2565BA Microarray Scanner System (Agilent). Data were analyzed using GeneSpring GX software (Agilent). The accession number for the microarray data reported in this paper is NCBI GEO: GSE120982.

Heat maps and principal component analysis plots were generated in the R-method. Gene Ontology (GO) enrichment analysis was performed using the ToppGene Suite (http://toppgene.cchmc.org/)(Chen et al., 2009).

Quantitative polymerase chain reaction assays

Total RNAs were extracted with the small intestines of mice of the indicated genotype at E18.5 and cDNAs were synthesized with the Revertra Ace qPCR RT Kit (Toyobo). Quantitative polymerase chain reaction (qPCR) analysis was performed with the 7500 Real-Time PCR detection system with CYBR green method of the target genes together with an endogenous control, murine *Hprt* with 7500 SDS software (Applied Biosystems). The primers used for qPCR were listed in Table S2.

Flow cytometry

After genotyping, three to four small intestines of the fetus of the same genotype at E18.5 were pooled and cut into small fragments and then digested with 1 mg/ml of collagenase (032-22364, Wako) in 10% FCS RPMI at RT for 30 min. Cells were passed through a 70 μm cell strainer, and single cell suspension was prepared. Cells were incubated with the indicated antibodies for 30 min. Fixable Viability Dye eFluor 506 (65-0816-14, eBioscience) was used to distinguish live cells from dead cells, and live cells were analyzed with the indicated antibodies.

Gating strategy for RORγt$^+$ ILC3s analysis was shown in Figure S6B. Briefly, CD45.2-positive but all lineage markers-negative cells were gated, and GFP-positive cells were analyzed by the expression of CCR6. The lineage markers used here were CD3, CD19, CD11b, CD11c, Gr-1, and TER-119. Data were obtained on a Fortessa (GE Healthcare) and analyzed by a Flow-Jo software (GE Healthcare).

Statistical analysis

Statistical analysis was performed by the two-tailed unpaired Student's *t* test or the one-way ANOVA test. $P < 0.05$ was considered to be statistically significant.

Supplemental References

Chen, J., Bardes, E.E., Aronow, B.J., and Jegga, A.G. (2009). ToppGene Suite for gene list enrichment analysis and candidate gene prioritization. Nucleic Acids Res *37*, W305-311.

Dannappel, M., Vlantis, K., Kumari, S., Polykratis, A., Kim, C., Wachsmuth, L., Eftychi, C., Lin, J., Corona, T., Hermance, N.*, et al.* (2014). RIPK1 maintains epithelial homeostasis by inhibiting apoptosis and necroptosis. Nature *513*, 90-94.

Eberl, G., Marmon, S., Sunshine, M.J., Rennert, P.D., Choi, Y., and Littman, D.R. (2004). An essential function for the nuclear receptor RORgamma(t) in the generation of fetal lymphoid tissue inducer cells. Nat Immunol *5*, 64-73.

Hao, Z., and Rajewsky, K. (2001). Homeostasis of peripheral B cells in the absence of B cell influx from the bone marrow. J Exp Med *194*, 1151-1164.

Matsumoto, S., Konishi, H., Maeda, R., Kiryu-Seo, S., and Kiyama, H. (2012). Expression analysis of the regenerating gene (Reg) family members Reg-IIIbeta and Reg-IIIgamma in the mouse during development. J Comp Neurol *520*, 479-494.

Newton, K., Sun, X., and Dixit, V.M. (2004). Kinase RIP3 is dispensable for normal NF-kappa Bs, signaling by the B-cell and T-cell receptors, tumor necrosis factor receptor 1, and Toll-like receptors 2 and 4. Mol Cell Biol *24*, 1464-1469.

Pfeffer, K., Matsuyama, T., Kundig, T.M., Wakeham, A., Kishihara, K., Shahinian, A., Wiegmann, K., Ohashi, P.S., Kronke, M., and Mak, T.W. (1993). Mice deficient for the 55 kd tumor necrosis factor receptor are resistant to endotoxic shock, yet succumb to L. monocytogenes infection. Cell *73*, 457-467.

Polykratis, A., Hermance, N., Zelic, M., Roderick, J., Kim, C., Van, T.M., Lee, T.H., Chan, F.K.M., Pasparakis, M., and Kelliher, M.A. (2014). Cutting edge: RIPK1 Kinase inactive mice are viable and protected from TNF-induced necroptosis in vivo. J Immunol *193*, 1539-1543.

Taniwaki, T., Haruna, K., Nakamura, H., Sekimoto, T., Oike, Y., Imaizumi, T., Saito, F., Muta, M., Soejima, Y., Utoh, A.*, et al.* (2005). Characterization of an exchangeable gene trap using pU-17 carrying a stop codon-beta geo cassette. Dev Growth Differ *47*, 163-172.

Zheng, Y., Valdez, P.A., Danilenko, D.M., Hu, Y., Sa, S.M., Gong, Q., Abbas, A.R., Modrusan, Z., Ghilardi, N., de Sauvage, F.J.*, et al.* (2008). Interleukin-22 mediates early host defense against attaching and effacing bacterial pathogens. Nat Med *14*, 282-289.